Master's Thesis by Olle Stenlund

# DESIGN AND MODELLING OF A CONTAINER FOR OPTIMAL FLOW RATE AND WASTEWATER PURIFICATION

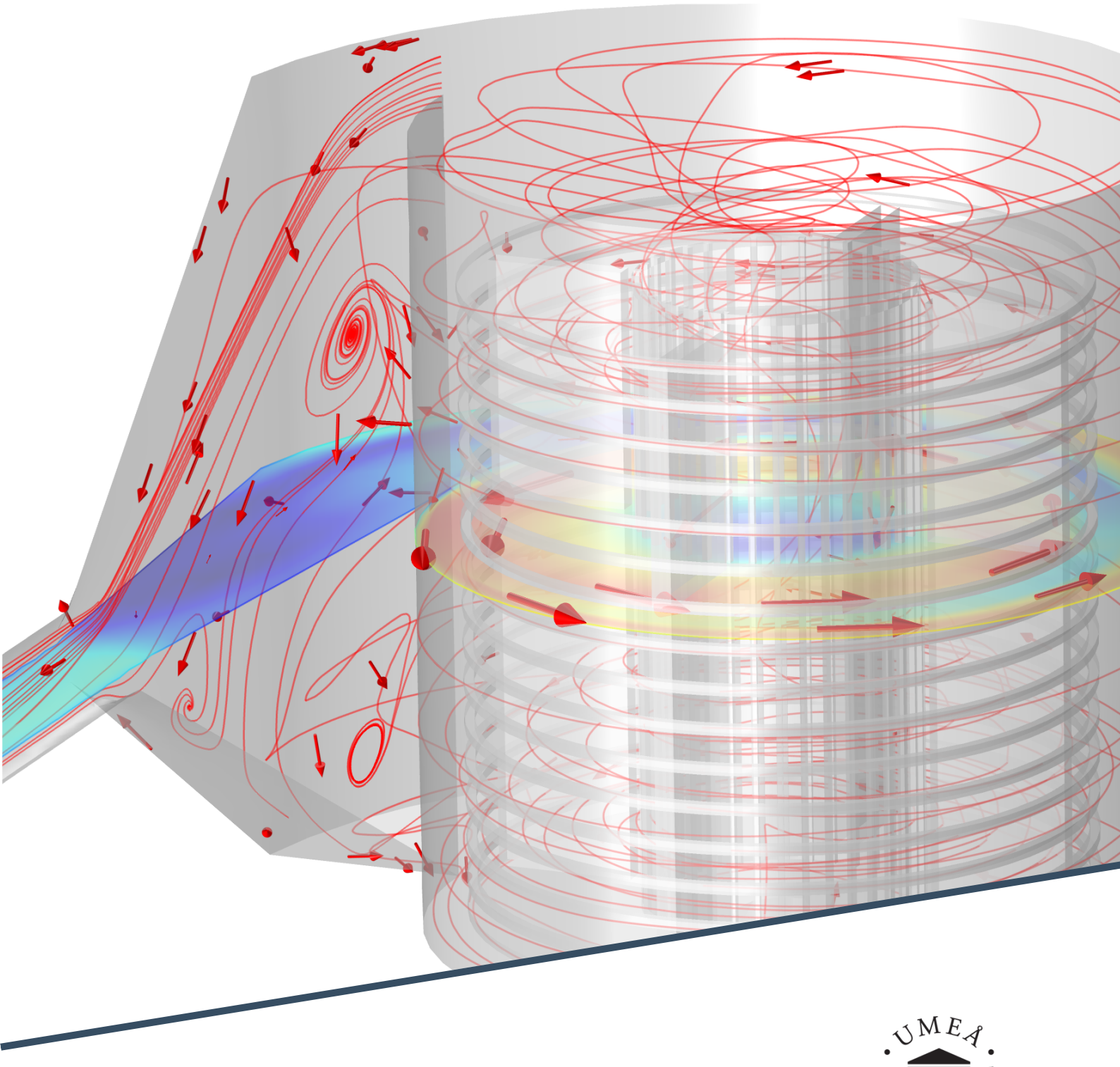

UMEÅ UNIVERSITY

MAY 2021

*Abstract*

Industries are becoming more aware of how they use water in their production process. In many cases, they release wastewater back into the water supply untreated, which can cause adverse side effects to the ecosystem. A sustainable environment requires efficient water purification. One approach to purify wastewater uses rotating bed reactors. An impeller filled with catalyst pellets that absorb the pollutants spins in the contaminated fluid. The inertial forces from the spinning impeller propel the contaminated water through the packed bed and purify it. In this study, we used one of these rotating bed reactors. However, the motors that drive these impellers can be bulky and may not be compatible with some tanks or environments. To solve this problem, we designed, constructed, and tested a container around the impeller that provides maximal outflow, using only the impellers pumping capability. We also developed a CFD simulation of the container to analyze the internal flows and forces. Because the flow generated by the rotating impeller displaces the fluid in a radial direction, the design works as a custom-made centrifugal pump. We constructed the container using plastic and wood with an outlet nozzle made of metal. The container's pump capability was around 2.5 liters per second when the impeller spun at 300 RPM. The developed CFD simulations gave a higher flow rate at 3.1 liters/second but overall helped shed light on the internal forces happening inside the container during high RPM testing. The design could generate a sufficient outflow of fluids, converting kinetic fluid energy to fluid pressure energy at the outlet, causing a pump effect. Overall, the design proved sturdy and could handle the forces occurring inside the container. The implementation of this design could allow industries to more efficiently and ergonomically utilize the purifying capabilities of the RBR in otherwise complex scenarios. By purifying wastewater before releasing it back into the water supply, we can take immediate action in achieving a sustainable environment.

# Contents

# 1

# *Introduction*

As the world moves towards a more Eco-friendly mindset, industries have become increasingly conscious of the effect their production has on the environment. It has become apparent that our available resources on this planet may be more limited than we initially expected; thus, more research has begun on achieving a more sustainable environment.

Water has always been a vital resource in modern industries. In the past, water was seen as a near-infinite resource. However, from 1950 to 2000, the total population went from 2.5 billion to 6 billion people [1]. The consequence of this significant increase is that the freshwater supply can no longer meet the ever-growing demand. In order to counteract this development, industries have become more aware of how they are using water as a resource and have started to develop ways to make their water usage both more clean and efficient to leave a smaller footprint on the environment.

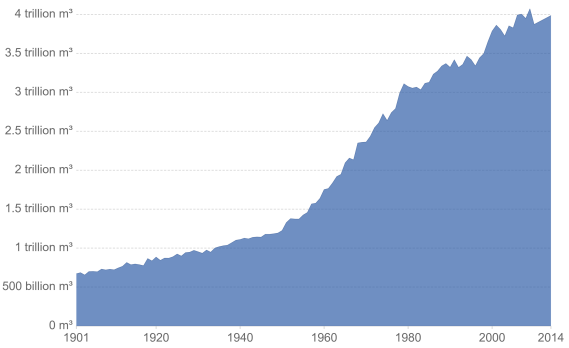


Figure 1.1: Graph over the global usage of freshwater per year [2]

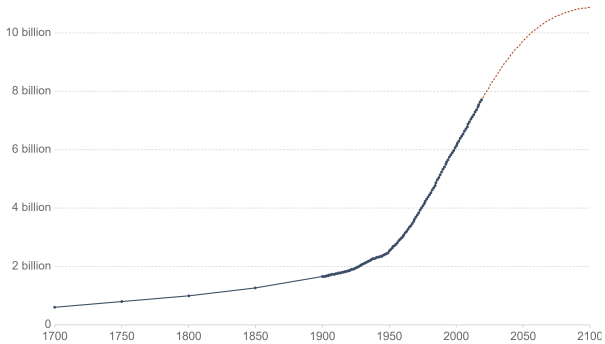


Figure 1.2: Graph over the population growth from 1700 to 2100 [3]

In a study done by Hannah Ritchie (2007), one can fully see how humanity's dependence on water has grown over the past century. Figure 1.1 displays the growing trend of freshwater usage. Figure 1.2 depicts the population growth of the world in the past three centuries. As one would expect, the usage of water is directly correlated to the increase in population. However, in Figure 1.2 one can also see

a prediction of how much the population will increase until the year 2100. One can safely assume that due to the high correlation between the two measures, the global usage of fresh water will also increase along with this same pattern. If this trend continues as expected, new methods and solutions need to be developed to ensure that our water usage remains sustainable and less taxing on the environment.

A consequence of industries using freshwater is that the water is often left contaminated after the production process. In a study by Jürgen Fönster (2014), roughly 40% of water used in European industries is left untreated [5]. A significant ecological hazard in today's world is when this untreated industrial wastewater is released into the water supply. This problem cannot be brushed aside if humanity strives to create an environmentally sustainable industry. A direct negative consequence of industries releasing their contaminated wastewater into the water supply is that it can be very harmful to livestock and agriculture, which depend on this shared water supply. In 2016, the University of California published a study on the extent that croplands are influenced by urban wastewater. In this study they found that 65% of irrigated croplands used water downstream from urban areas where many industries did not treat their contaminated water before releasing it back [6]. If this trend continues unaddressed, humanity will slowly but surely be pushed into a corner where our industries have caused so much damage to the ecosystem that they no longer can provide humanity's growing demand for food and clean water.

The water purification process for industrial wastewater demands quite a lot of energy. Over 30% of the costs in wastewater treatment facilities go to the energy supply, and studies even show that these facilities can require roughly 3% of an entire country's electrical output [10]. Therefore these purification processes are in dire need of some optimizing and innovations. Thus, due to the demand for freshwater increasing steadily, more research is going into contaminated wastewater remediation.

## *1.1 Project background*

The project has its origins in this remediation process where one purifies contaminated water as efficiently as possible to be reused. This process relies today on utilizing mixer tanks filled with contaminated water and coagulants that absorb the unwanted chemicals from the water. This process can be quite time-consuming and require much power. To counteract this problem, SpinChem® has developed a device called the Rotating Bed Reactor (RBR). This flexible invention optimizes the purification process by combining the coagulant material (ion exchange resin) and mixer itself. This design is somewhat reminiscent of a so-called packed-bed reactor, where one wants the

liquid to travel through a bed of densely packed solid phase.

There are a couple of ways to purify water using an RBR. Most commonly, one can submerge it directly into a tank with contaminated wastewater and then, with the help of a motor, spin the RBR purifying the water inside the tank. However, these motors can be quite cumbersome and may not easily fit large tanks or tanks with unique shapes; the tank may not even have a big enough hatch to fit a suitable RBR. To solve this problem, one may put the RBR inside its own container and connect this custom-made container with the tank containing contaminated wastewater. Then, by spinning the RBR in this container, it will act as a pump and circulate the wastewater in a closed loop. A schematic of this process can be seen in figure 1.3.

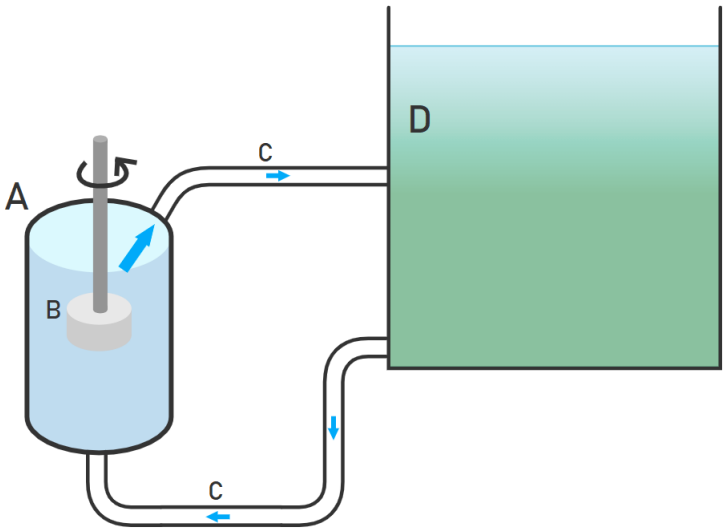


Figure 1.3: Experimental setup of the project. The components are as follows, *A* is the RBR container, *B* is the RBR module, *C* are the pipes connecting the two containers and *D* is the container with the contaminated water.

This project aims to create an optimized RBR container, which will as efficiently as possible pump the water in this closed system. The flow rate between the two tanks should be as fast as possible using only the flow caused by the RBR, i.e., no external pump should be used to transport the water. This container should be designed, built, and tested to check its effectiveness. Removing the need for an external pump and designing a container that allows for a more hydrodynamic flow should result in the water purification process becoming both more energy and time-efficient. If it is proven successful, this design may be utilized to purify of contaminated water from textile industries or water used in other various industrial processes. Coinciding with the design and building phase, a *Computational Fluid Dynamics* (CFD) simulation of the water flow inside the container will also be developed and analyzed.

The impeller and purifier for the closed system is the SpinChem® developed RBR S14, which can be seen in figure 1.4 and 1.5. The flow profile of the RBR S14 is similar to that of a Rushton impeller.

Figure 1.4: Picture of the Rotating Bed Reactor S14, which is to be used for this project.

Figure 1.5: The inside of the RBR S14.

To summarize, the project will be divided into a set of steps. Firstly a design phase, then a construction phase, and lastly, a testing phase.

The S14 is designed as both a mixer and stirring impeller; this means that its initial purpose is to be lowered in a tank with contaminated water, let it spin inside that tank until the water is purified, and then take it out. By understanding the flow caused by the S14, one can apply that knowledge into developing a container with high efficiency convert the rotation of the impeller into an outflow of the container.

The construction of the container will indubitably be the most time-consuming part of this project. A delicate balance of precision and speed needs to be applied when building the container, as one can easily spend much time polishing minor problems in the design that gives little to no effect on the actual results. Therefore one must plan as to how the construction should be conducted. An essential part of the construction phase is to remain flexible, as the initial design will undoubtedly go through several adaptations to solve newfound problems. The construction of the container will thus consist of building a prototype of the designed container.

To get a better idea of the effect of the design, CFD simulations will be done. These will be compared to one another to see how closely the CFD simulation mimics reality. Due to their simplicity, the materials chosen to build the container were wood and plastic. During the testing phase, the main parameter to be examined is the flow rate. The motor controlling the spin of the impeller can be adjusted to change the rotational speed. The values recorded from the tests should show the overall effectiveness of the chosen design; it will also aid in providing some insight for further optimizations.

The CFD simulations done alongside the construction will be used as a sort of benchmark, to more easily understand what kind of forces one can expect to occur inside the container. By analyzing the results from the simulations, one may find otherwise hidden flaws in the container and thus prepare in advance to solve these problems. The simulation, if done correctly, will also give an idea of what results one can expect from the actual real-life testing.

# 2

# *Theory*

This project consists of designing and constructing a water pump; this theory chapter will focus on the hydrodynamics involved and how the impeller propels the liquid inside the container. The theory behind the CFD simulations will also be introduced in this section.

## *2.1 Theory concerning the container shape and design.*

In order to find a proper design for the container, one needs first to understand what type of flow will occur due to the impeller used. For all intents and purposes, the final chosen design of the container will wholly depend on the hydrodynamics of the impeller.

As seen in figure 2.1, there are many different types of stirring impellers, each having a unique impact on the flow inside the container. When analyzing the flow caused by impellers, one most often talks about either *radial-* or *axial flow*. Radial flow describes a type of flow where the rotating impeller drives the fluid to move perpendicularly to the impeller shaft, i.e., towards the mantle walls of the container. On the other hand, axial flow describes a type of flow where the impeller drives the fluid towards the top or bottom of the container. These types of flow are demonstrated in figure 2.2.

As the RBR-S14 has a similar flow pattern as a Rushton impeller, which is the disc flat blade impeller that can be seen in the middle of figure 2.1. The Rushton impeller has a radial flow profile similar to that of the top in figure 2.2. There are many pumps that utilize impellers with a radial flow profile; one example of such a pump is known as a *centrifugal pumps*.

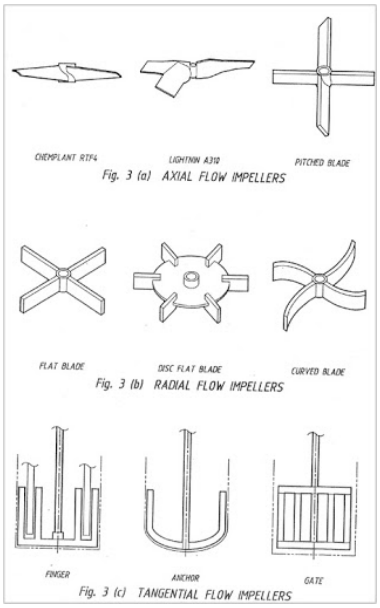


Figure 2.1: Figure depicting several different types of stirring impellers. [11]

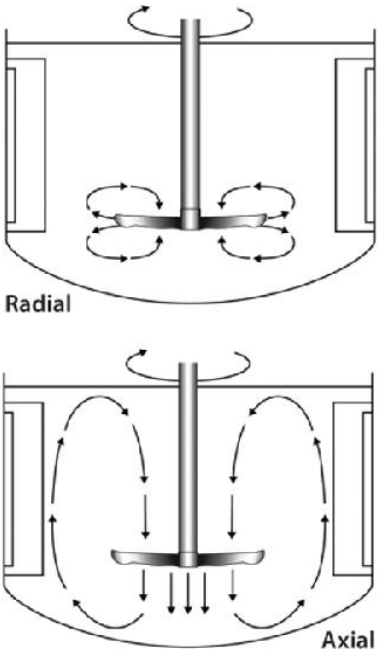


Figure 2.2: Figure depicting the flow profiles of radial- (top) and axial flow (bottom).[12]

### 2.1.1 The Centrifugal Pump

The centrifugal pump has been in use since the 17th century and has proven to be an effective way to transport liquids. The basic principle of a centrifugal pump is reminiscent of most pump systems. By setting spin to an impeller with the help of a motor, the energy from this rotation will then be transferred into the fluid, setting it into motion. In a centrifugal pump, the inlet is located, that the liquid is entered through the center of the impeller. Due to this and the shape of the impeller, the liquid will be forced radially outwards towards the pump's casing, increasing both pressure and velocity in the process. The casing, or volute as it is also called, has a cross-sectional area that is increasing towards the outlet of the pump. This shape is similar to a logarithmic spiral. The consequence of this shape is that the fluid will lose velocity as it moves towards the outlet, but it will thus gain pressure. This rule applies in incompressible flows, which refers to a type of flow where the fluid density remains constant. This conversion from velocity to pressure is more commonly known as the *Bernoulli's Principle*.

Bernoulli's Principle, which is often referred to as the *conservation of energy principle*, states that inside an isolated system, the total energy must remain constant and conserved over time. The general energy equation or *Bernoulli's equation* in an incompressible flow is as follows

$$p_1 + \frac{1}{2}\rho {v_1}^2 + \rho g h_1 = p_2 + \frac{1}{2}\rho {v_2}^2 + \rho g h_2. \tag{2.1}$$

$p$ is the pressure, $v$ is the velocity, $\rho$ is the fluid density, $g$ is the acceleration due to gravity and $h$ is the elevation. This equation describes the energy inside a fluid at two different points on the path, which must be equal due to the conservation of energy. In the context of a centrifugal pump, the change from $h_1$ to $h_2$ will depict a change from a small area to a region of the increasing area. This change will cause the kinetic energy to be converted into pressure energy [13]. Utilizing the knowledge from Bernoulli's principle, one can get an idea of what makes a centrifugal pump so effective. If the inlet has a very low pressure compared to that of the outlet, a suction will occur between these two points, effectively causing a pumping effect. It is precisely this principle that makes centrifugal pumps so effective that they have been in use for centuries.

With a basic understanding of the physics involved in the flow, let us look at the components that a typical centrifugal pump is composed of.

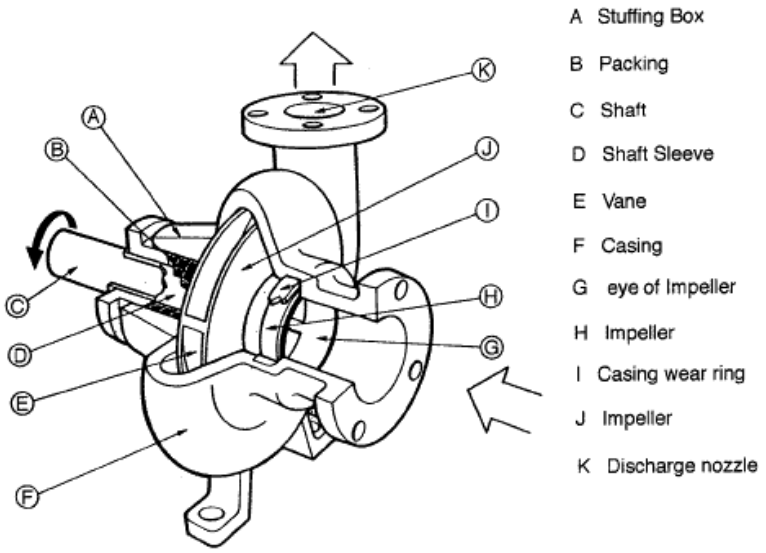


Figure 2.3: Figure depicting the components in a standard centrifugal pump. [14]

This figure contains most of the terminology that will be used during the construction of the container; the primary points of interest are:

- **C**: The shaft which put the impeller into a rotating motion. It is connected to a motor.
- **E**: Vanes on the impeller are the blades that give the fluid its kinetic energy.
- **F**: The casing is the container which encompasses the impeller and the fluid. The shape of the casing will cause the kinetic energy of the fluid to be converted into pressure energy.
- **G**: The eye of the impeller is where the inlet of the pump is located. It is positioned in such a way that the liquid enters through the center of the impeller. The rotation of the impeller together with the vanes will then cause the fluid to be directed radially towards the outer wall of the container.
- **J**: The impeller is the main component in setting motion to the liquid. It has several vanes to direct the flow of the fluid. It is connected to a shaft which is in turn connected to an external motor.

The ever-growing cross-sectional area inside a centrifugal pump is often reminiscent of a logarithmic spiral, which is also known as a growth spiral [17].

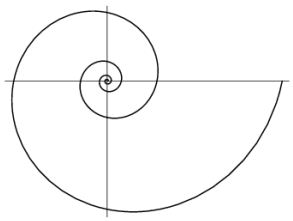

Figure 2.4: Figure depicting the logarithmic spiral. [17]

Logarithmic spirals, as seen in figure 2.4 can be found almost everywhere around us, from seashells to spiral galaxies. The polar equation of this type of spiral is

$$r = ae^{b\theta},$$

where $r$ is the distance from the origin, $a$ and $b$ are arbitrary constants and $\theta$ is the angle from the x-axis. This function can be expressed parametrically as

$$\begin{aligned} x &= r\,cos\theta = a\,cos\theta\,e^{b\theta} \\ y &= rsin\theta = a\,sin\theta\,e^{b\theta}. \end{aligned} \tag{2.2}$$

By utilizing these equations, one can plot a suitable shape for the mantle of a centrifugal pump.

As discussed earlier, a vital detail in the inner workings of a centrifugal pump is the effects happening at the inlet and outlet. As the pressure is increased at the outlet due to the conversion of energy, the pressure here will be larger than at the inlet. This pressure differential will cause suction at the inlet. This effect is integral in causing the characteristic high flow rate of centrifugal pumps. This pressure difference may also lead to a phenomenon known as *cavitation*. Cavitation is the process when the pressure of the liquid at the inlet and impeller is so low that it dips below its vapour pressure. This low pressure will cause the liquid to start boiling, and thus bubbles will begin to form. As these bubbles go from a low-pressure area (inlet) towards a high-pressure area (outlet), they will begin to implode; this phenomenon may damage the pump components. The cavitation phenomenon in centrifugal pumps can be more easily visualized in the figure below

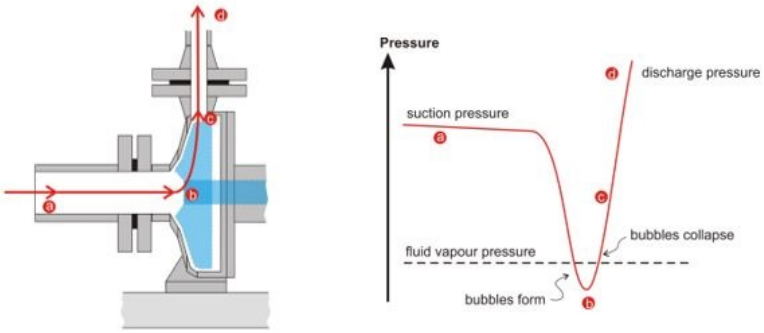


Figure 2.5: Figure depicting pressure difference and resulting cavitation inside a centrifugal pump. [16]

In figure 2.5 (left), one can see how the liquid is transported from point $a$ to point $d$ through a centrifugal pump, and on the right, one can see the pressure levels in those respective points. As the liquid travels from the inlet, a considerable drop in fluid pressure occurs. Due to this, depending on the temperature of the liquid, it can drop below fluid vapour pressure and begin to boil. The bubbles caused by this will then travel towards the outlet where the pressure is drastically higher, causing the bubbles to implode.

## 2.2 CFD Theory

This section will cover the theory utilized in the CFD simulations.

### 2.2.1 Computational Fluid Dynamics simulation

To put it simply, these types of simulations are a way of numerically analysing the behaviour of fluids in motion. These analyses can have complex interactions such as the interaction between two fluids with different viscosities, fluid interacting with solid matter, and fluid interacting with gasses. However, the more complex one's model becomes, the more computational power is required to simulate it. When one thinks about it, fluid dynamics are everywhere in our daily lives, from the aerodynamics of the air drag on one's car, to the hydrodynamics when swimming in the ocean. CFD is a handy tool to predict the otherwise chaotic behaviour of fluids in different circumstances.

A thing to understand is that the mathematics and physics behind fluid dynamics are both quite laborious and challenging. This is why computers most often tackle these problems. The most common type of equation solved for in fluid dynamics are called the Navier-Stokes Equations [18]. These equations are a way to express the three-dimensional motion of viscous fluids mathematically. With the assumption of Newtonian and incompressible (constant density) fluids, the Navier-Stokes equations have the following appearance

$$\begin{aligned} \Delta \cdot \vec{u} &= 0 \\ \rho \frac{D\vec{u}}{Dt} &= -\Delta p + \mu \Delta^2 \vec{u} + \rho \vec{F} \end{aligned} \tag{2.3}$$

The first part in equation 2.3 is the continuity equation for the conservation of mass, here $\vec{u}$ refers to the velocity vector of the fluid. In layman's terms, this states that the fluid can change shape, but the total mass remains unchanged from start to finish.

The second part is a set of three differential equations, which de-

scribe the conservation of momentum in the system. On the left side, one has an equation that can be explained as Newton's second law for fluids. If the volume is the same in the fluid, one can say that the mass and density are the same; in this equation, $\rho$ is the density of the fluid.

The first term of the right-hand side, $\Delta p$, is the fluid pressure gradient. It depicts the difference in the pressure in the container. The second term, $\mu\Delta^2\vec{u}$ depicts the viscosity of the fluid. The final term, $\rho\vec{F}$ depicts the external forces; this will usually be the gravitational forces on the liquid.

To this day, there is no general analytical solution for this equation that can work for every type of situation. However, if the geometry is simple, and one knows the conditions for all the boundaries in this simple geometry, a solution to the equations can be found. This notion is the basic principle of how CFD solves the Navier-Stokes equations. It takes a complex geometrical surface, splits this up into many smaller, more simple surfaces, then solves the Navier-Stokes equations on these by simple computational brute force. These tiny surfaces are called cells, all of them combined is called a mesh. Each of these cells interacts with the neighboring cells. By setting known values at the boundaries along the mesh edges, the computer starts a brute force iteration process where it tries to balance all the cells and edge boundaries until a good solution is found. Now, this iterative process will continuously try and improve the solution; when the solution has reached an acceptable level where the error is low enough, the simulation is completed; this is more commonly known as convergence.

### 2.2.2 *Turbulent flow, k-$\omega$*

When one wants to simulate a more complex and chaotic flow in CFD, it would be wise to utilize turbulent flow models. The physics and mathematics concerning these models are pretty extensive, so this section will only briefly cover the inner workings of one specific model which was used in this project, the turbulent flow k-$\omega$ model [19]. These models augment the Navier-Stokes equations in 2.3 with an added turbulence eddy viscosity term. An *eddy* is the swirling that can occur in the flow, causing a space devoid of downstream-flowing fluid. As the name states, the k-$\omega$ model solves for two variables. $k$, the turbulence kinetic energy, and $\omega$ which is the specific dissipation rate of kinetic energy. This model can utilize wall functions, which define how the fluid behaves near walls; this is especially useful when dealing with turbulent fluids. The $k-\omega$ model was chosen for the simulations in this project as it can be extra helpful in cases where the flow exhibits strong curvatures.

# 3

# *Methodology of the design*

This chapter will cover the design and construction phase of both the actual container and the CFD simulations. My plans and how I executed them will be motivated so one can easily follow my thought processes.

## *3.1 Container Design planning*

The design of the container did not have to abide by many specific requirements, the main one being that it had to utilize the RBR-S14 as its impeller. This meant that there was much leeway in experimenting with different types of designs. To narrow down the process of finding a suitable design, we set a framework of requirements that the container ought to meet. They are as follows:

- Focus of the outflow and pumping capability.
- Watertight.
- Try to avoid making it too bulky.
- Ensure it is compatible with the equipment at the workshop (such as mixer motor, hosing, and so forth.)
- Try to make it as sturdy as possible so that it can endure several tests at high RPM.
- Complex enough to show promise, but simple enough to be able to build within the allotted time.
- Incorporate relevant sensors in the container to measure its effectiveness.

By knowing that the flow caused by the impeller is similar to that of a Rushton Impeller, I could begin brainstorming potential designs that ought to complement this flow profile and result in a good outflow.

As the flow will go radially outwards from the impeller towards the walls of the container, a fitting design would be something that utilizes this flow and redirects it out. So I set out to the drawing board and begun sketching my initial ideas.

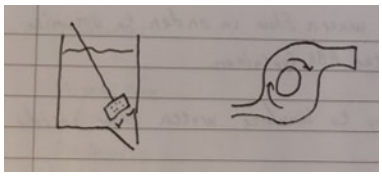

Figure 3.1: Sketch of the flow patterns, left figure depicts how one could utilize setting the impeller at an angle together with axial flow to throw water to the bottom. The right picture depicts a radial flow pattern.

Firstly I thought of how different shapes alter the hydrodynamics of different flow patterns. As seen in figure 3.1 I thought that if one has an impeller that instills a rotation upon the liquid, one ought to have a container with a shape that is harmonious with this flow, i.e. a shape with as little resistance as possible on the fluid. Therefore I developed the sketch in 3.2, which then gave me the realization that if one wants to create a high outflow from a radial flow pattern, why not just utilize a similar shape to that of a *centrifugal pump*.

Figure 3.2: A further developed sketch on a potential container built around a radial flow.

### 3.1.1 *Centrifugal pump design.*

From the points mentioned earlier, the basic design was chosen to be something akin to a centrifugal pump. These pumps utilize an impeller with a radial flow pattern, and a specific container design optimized around this flow to create both suction from the inlet and fast flow out of the outlet. The composition of a centrifugal pump can be seen below

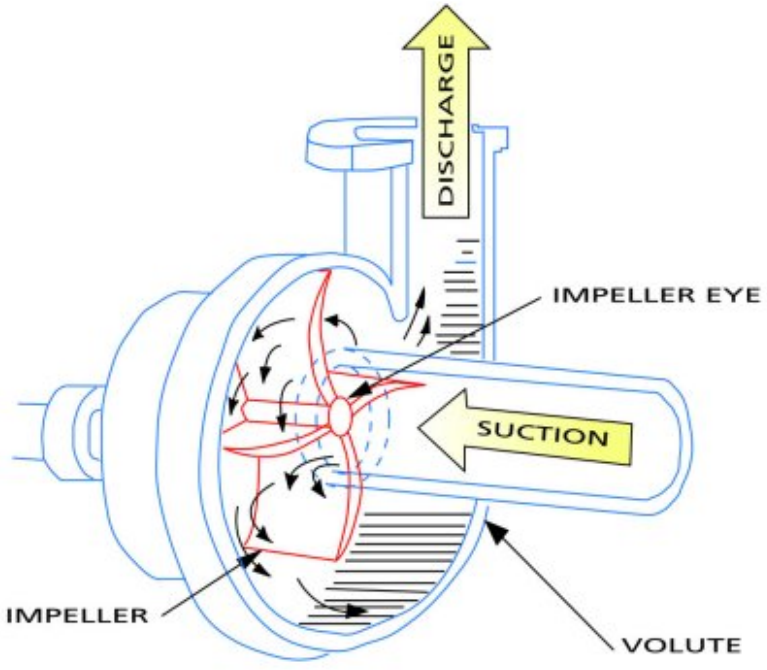


Figure 3.3: Cutaway of a centrifugal pump. [15]

Here in figure 3.3 one can see the basic principle of the inner workings inside a centrifugal pump. The idea is that the positioning of the inlet, the shape of the casing together with the impeller causes both a discharge and suction to occur, i.e. a pumping effect.

Now with this knowledge, I could continue to build upon the design of the container. The sketch in figure 3.2 was thus further developed into the following sketches.

Considering that centrifugal pumps are often very enclosed and tight around the impeller, as can be seen in figure 2.3, certain compromises had to be done to the design. As one can see in figure 3.4 the housing would thus resemble an elongated centrifugal pump that could adequately fit the cylindrical shape of the impeller. However, one can quickly see the flaw in figure 3.5. The water displacement would be pretty low with this design since the outlet is somewhat constricted at the bottom. A solution to this would then be to create an elongated centrifugal shape that can fully encompass the impeller.

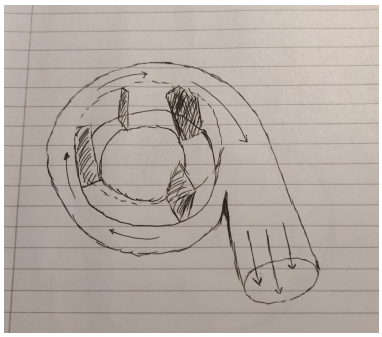

Figure 3.4: The inside of the container.

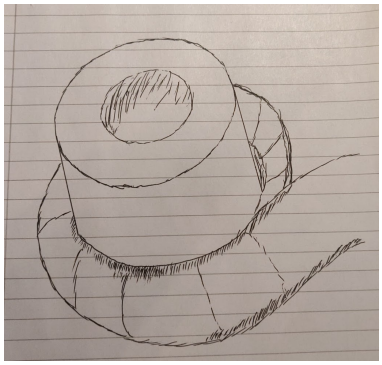

Figure 3.5: The outside of the container.

## 3.2 *Container design development*

With the sketches done and a solid design idea in mind, 3D modelling of the container could start. By creating a CAD model, it would be far simpler to visualize the individual components of the container. This CAD model would work both as a blueprint for when the construction began and utilized in the CFD simulations. When modelling the container, the initial steps to follow were,

- Step 1: Find a shape for the mantle of the container.
- Step 2: Model it in such a way that the impeller can easily fit.
- Step 3: Model a fitting nozzle for the outlet.
- Step 4: Optimize the design.

So for starters, a suitable shape for the mantle had to be found. The casing in centrifugal pumps often takes on a spiral shape, more specifically, a logarithmic spiral. Thus by utilizing equation (2.2), together with these parameters:

| | |
|---|---|
| a | 1 |
| b | 0.1061 |
| $\theta_{initial}$ | 15.894 deg |
| $\theta_{final}$ | 22.088 deg |

the following spiral was made.

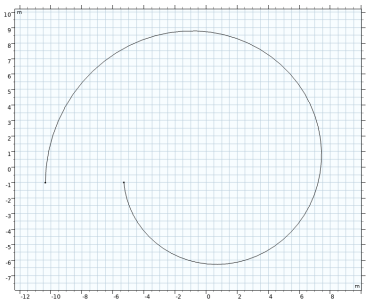

Figure 3.6: Logarithmic spiral to be used for the initial design.

This spiral in figure 3.6 will be the initial backbone of the entire container. Naturally, it took some experimenting and finessing with the parameters to get them just right. The parameters of the spiral were set so that the starting point and endpoint would be level. The gap between these two points is where the outlet will be; it was also made sure that the spiral had such a shape that the impeller could

fit inside. With this, the design could go on into 3D by setting the spiral as the floor and then extruding this shape outwards.

In figure 3.7 one can see the first iteration of the design. However, with this, the actual design for the container started getting more and more concrete. The container would be a custom-made centrifugal pump casing that can fit the impeller. Now the water has to go somewhere; therefore, a suitable nozzle must be modelled for the outlet. The initial idea was to create a type of choke that would press the water into some hosing without causing too much resistance in the flow.

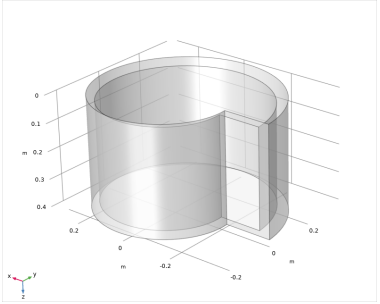

Figure 3.7: Mantle and floor created from the logarithmic spiral.

This temporary nozzle design in figure 3.8 ought to more efficiently direct the water towards the outlet. The circular tubing has a radius of 2 inches and will hopefully be enough to sustain a good outflow.

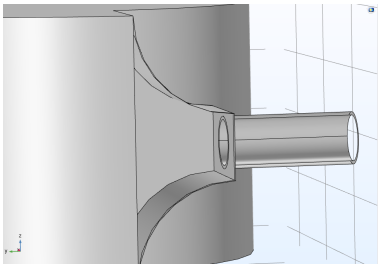

Figure 3.8: Updated nozzle design cutaway.

To better visualize how well the impeller fits inside the design, a 1:1 scale model of the impeller was inserted. In figure 3.9 one can easily see that the impeller fits nicely inside the current design. Here one can also get an idea of the motivation of where to position the impeller inside the container. In order to make the most use of the logarithmic shape, the impeller should be located as close to the inner wall as possible (inner wall meaning the wall nearest the starting point of the spiral). By positioning it here, the water will flow along the continuously increasing cross-sectional area. Thus the kinetic energy of the fluid will be converted to fluid pressure according to equation (2.1). While the current design is rather simplistic, modelling it did help to shed light on flaws that may have otherwise been overlooked.

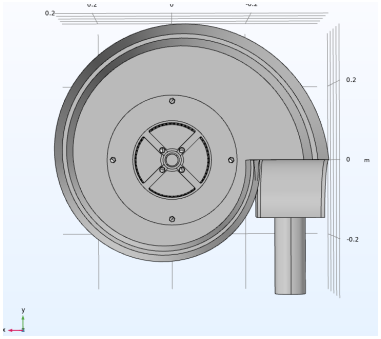

Figure 3.9: Initial design of the container with the impeller inserted.

The most apparent flaw recognizable at this point is the size of the container; it is simply a bit too big. One generally wants the pump's casing to be pretty tight around the impeller, so as not lose too much kinetic energy in the fluid. In figure 3.9 one can see there is much dead space between the impeller and the impeller and the walls of the container. Having much dead space means that the pressure gradient between the inlet and outlet will be more evened out, i.e., the overall energy in the water will be dissipated. Having a more compact container will cause the water to have a higher energy density and a better outflow. As we could not change the size of the impeller, the problem was thus to find a way to make the container more compact.

To solve this problem, a new spiral was made with a smaller area to better encompass the impeller. The new spiral parameters were as follows:

| | |
|---|---|
| a | 4.5 |
| b | 0.047746 |
| $\theta_{initial}$ | 28.274 deg |
| $\theta_{final}$ | 34.558 deg |

which resulted in this spiral.

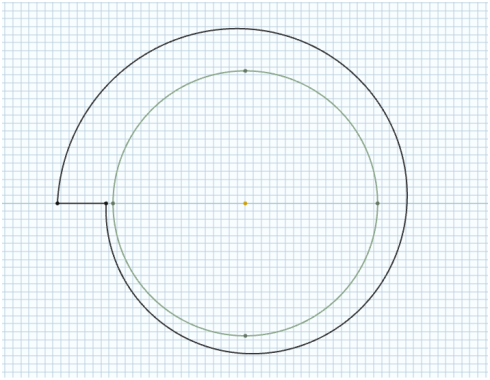

Figure 3.10: The updated logarithmic spiral with reduced area.

This shape had a much smaller area and thus encompassed the impeller more tightly. In figure 3.10 the green circle represents the impeller. This shape would be a suitable choice, but it has one major flaw, the outlet. The outlet can only be 60mm wide with this shape, which is way too narrow when one wants a good flow rate. In order to solve this issue, a compromise was made. The first 270° (starting from the inner wall) of the spiral in figure 3.10 was plotted, but the last 90° was done with a circular arc which allowed for a wider outlet; with this optimization made, the following shape was acquired

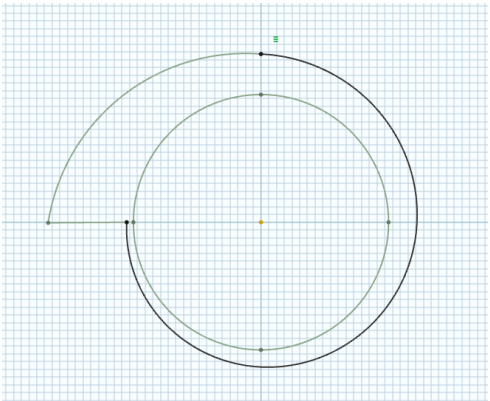

Figure 3.11: The optimized logarithmic spiral with a smaller area and wider outlet.

The spiral seen in figure 3.11 is the final iteration of the mantle design, where the outlet now has a width of 100mm. The design was determined to be good enough to be utilized in the final design of the container. With the new, optimized shape, the more proper 3D CAD model of the container could start.

First and foremost, the height of the container had to be determined. With the impeller having a height of 310mm, and the shaft coupling being around 50mm, I decided to give the mantle a height of 400mm. That way, there will be a bit of breathing room for the shaft and inlet, and some space available for impeller adjustment.

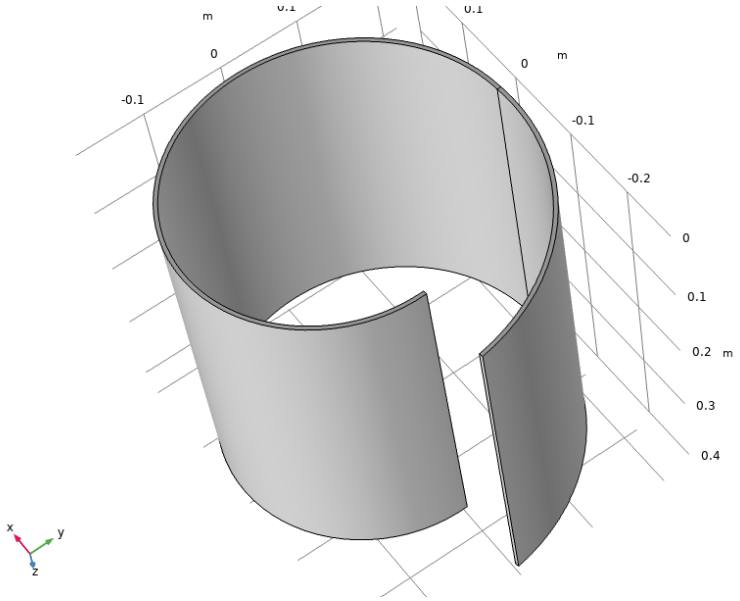


Figure 3.12: The mantle of the container.

This mantle, seen in figure 3.12, would indubitably be the most crucial part of the container. It would both have to be structurally strong enough to withstand the forces inside and have a cross-sectional area that increases in such a way that the kinetic energy will convert into pressure energy at the outlet. From these CAD models, accompanying blueprints were developed for each container component; these blueprints can be found in the appendix of this report. These blueprints were used as a sort of baseline for the design. In blueprint 31 one can see the dimensions used for the spiral mantle. As the spiral is grew, it was quite challenging to try and make a blueprint for depicting this properly, so the radii from the spiral to the center were written out from each quadrant. The arc length of the spiral is 1304mm, and the thickness was set at 5mm. However, this thickness was prone to change depending on what material one wants to use for the construction.

Next up in the design was the top lid. This component has two main parts: the top lid and the top lid cover, but for starters I will focus on the top lid. The idea was for the top lid to keep the same shape as the spiral to not make the container too bulky but also thick enough to allow for an indent for the top lid cover. Thus the resulting design was a 15mm thick top lid, with a 5mm deep indent for the accompanying cover and a hole cut out in the proper location where the impeller is lowered. The indent will have a couple of bolts sticking up, where one can fasten the top lid cover. A fitting gasket

will also be placed on this indent to create a good seal and prevent leaks.

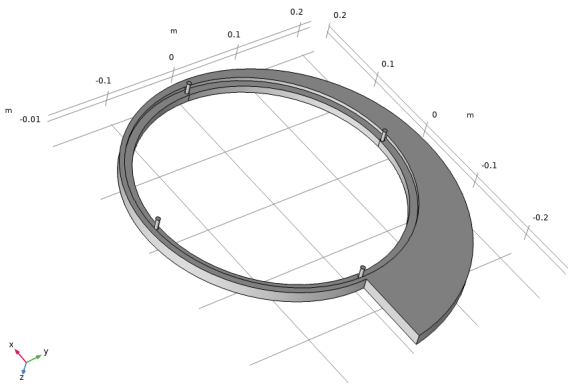


Figure 3.13: The top lid of the container.

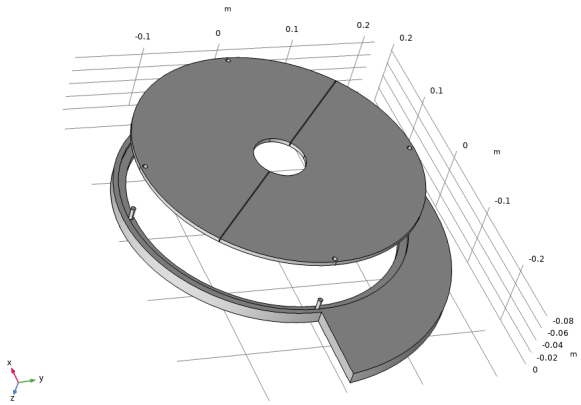


Figure 3.14: The first design of the top lid cover.

In figure 3.13 one can visualize the idea I had for the top lid. The lid retains the shape of the spiral, has a large enough hole to fit the impeller, and an indent with bolts used for fastening the cover. In blueprints 32 and 33 one can see the dimensions of the top lid. Now for the second component in the top lid, the cover. At first, I guilelessly had the simple idea to put a circular disk on the top lid with holes at the right places to fit bolts on the top lid and tighten it with wing nuts. This design can be seen in figure 3.14. However, I quickly realized that this design would leave an open hole for the shaft, which could be pretty tricky to seal. As the shaft is expected to reach up to 300RPM in the experiments, one can imagine a lot of water flying out of this hole and fitting a perfect sealing gasket around the shaft and top lid cover could prove quite cumbersome.

To solve this issue with the top lid cover, I decided to take inspiration from the appearance of the mixer motor and its design. This mixer motor had an accompanying top lid cover fastened on it designed for another container. This cover provided a good seal around both the shaft and its own container, very similar to what I needed for my design.

Here in figure 3.15 one can see the cover used for another container. From this cover, I realized that something similar would be a suitable design for my top cover. Having a cover that is bolted directly to the motor means that it would provide both a good seal from the outside and stability as the container would be directly fastened to the mixer motor. A benefit of this is that if potential vibrations occur during high RPM testing, the container will vibrate together with the shaft and mixer motor. This way, I would not need to worry about the impeller hitting the walls of the container. With this in mind, the following sketch was developed.

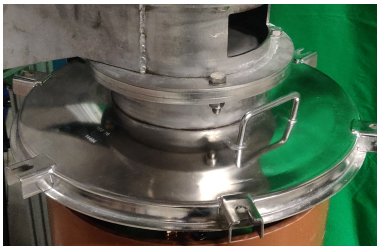

Figure 3.15: A top lid cover used for another container at the laboratory.

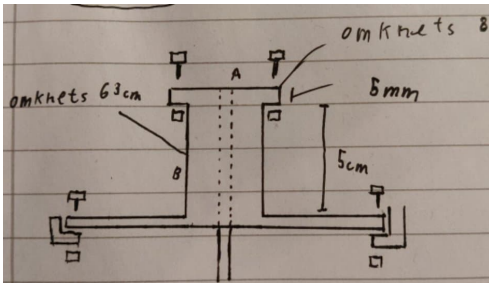


Figure 3.16: Sketch of the proposed design for the top lid cover.

In figure 3.16 one can see the initial design proposed for the top lid cover. In the sketch, I have pictured the height of the neck, which is to be connected to the mixer motor with bolts. With this sketch, I created the following model.

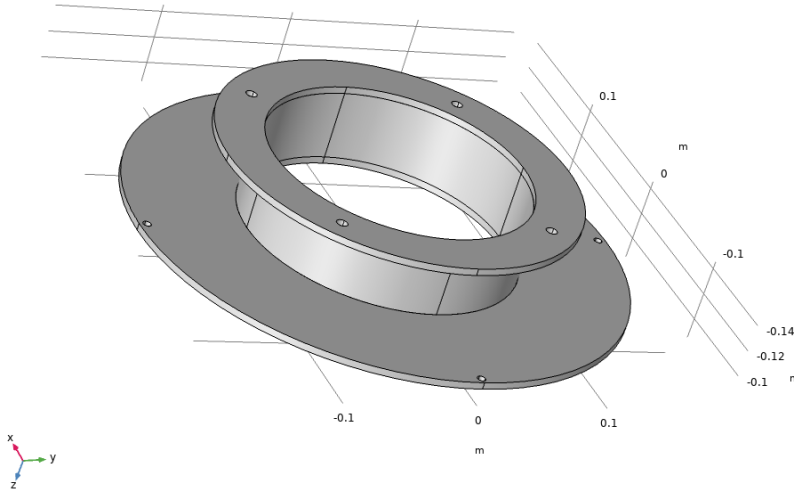


Figure 3.17: Final design of the top lid cover.

The neck part of the cover in 3.17 needs to be a bit elongated since otherwise, the container will collide with the supporting arm that holds up the mixer motor. This support arm can be seen in the top left of figure 3.15. Naturally, the holes for the bolts connecting the mixer motor and the cover were also aligned to fit. In appendix 34 and 34 one can see the blueprints for the top lid cover. Again, these schematics would be considered flexible and prone to changes during the construction phase but should suffice as a good baseline.

Now for the bottom part of the container, it is here where the inlet for the container will be. It is of high importance that this inlet is positioned directly below the center of the impeller. The consequence of such a misalignment is an uneven water flow, worsened suction effect, and overall a more turbulent flow pattern at the inlet. Besides that detail, the overall shape of the bottom lid would be similar to that of the top lid.

In figure 3.18 one can see the basic design of the bottom lid. The cylindrical piece near the center depicts the inlet. The inlet component would most likely need to be store-bought. Therefore in the 3D model, it was just kept as a cylinder to showcase potential size and location. The diameter of the inlet was chosen at around 2.5 inches since it is the same dimension used for a potential fitting inlet I found at a store. However, this dimension is flexible depending on if a better inlet is found. The blueprint for the bottom lid can be seen in appendix 36.

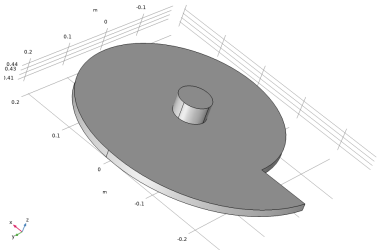

Figure 3.18: Design of the bottom lid.

The next component to be addressed is a straightforward one. It is a sort of attachment placed at the base of the outlet on the container. The purpose of this piece is to act as a fastening point for the outlet nozzle. Thus, the basic idea was to create a rectangular frame that fit perfectly not to create any unnecessary resistance.

In figure 3.19 and appendix blueprint 37 one can visualize the simplicity of the frame. While it is not a very complex component, it is an important one, as it acts as the bridge between the container and the outlet nozzle. The idea is for the nozzle to be welded upon this frame along the edges. The width of the edges in this frame is designed around using metal as the material. However, if one were to use something like wood, the edges would have to be thicker to allow for screws.

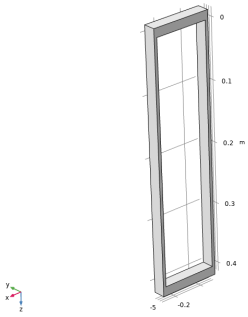

Figure 3.19: Design of the outlet attachment frame.

The main idea for the nozzle was to have something that smoothly goes from a rectangular shape to a circular shape. The design for the new nozzle took its inspiration from the initial design seen in figure 3.8. The idea was to create the transition between the rectangular connection to a circular outlet which was as seamless as possible to avoid unnecessary friction.

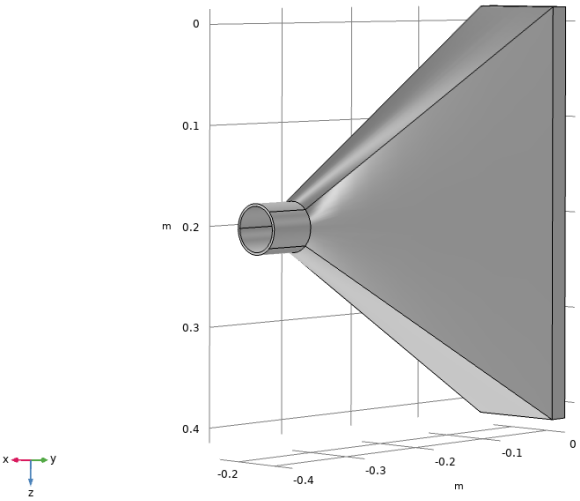


Figure 3.20: Design of the rectangular to circular transition nozzle.

Here in figure 3.20 one can see the proposed design for the outlet

nozzle. As the hosing used at the laboratory had a diameter of 2 inches, the circular outlet ought to have the same diameter as this. It was essential to make sure the surfaces in the nozzle would direct the flow towards the outlet. Therefore, by using a loft command, the transition from rectangular to circular became sufficiently smooth..

This design should prove simple enough to build and sufficient enough to direct the water towards the outlet. However, an immediate notable concern is the bottleneck caused by the nozzle. One would preferably want the difference between the rectangular area and the circular area not to be too big, but since the available hose has a diameter of 2 inches, it was a necessary compromise. A probable side effect of this bottleneck is that the water might bounce on the surface and create several vortices, which will cause the water to flow in the wrong direction. However, the design for the outlet nozzle was stopped at this stage, i.e., no blueprints were made for this component. The reason for this was that I found a company that specializes in ventilation equipment that already had a rectangular to circular nozzle that shared more or less the same appearance as the nozzle I needed. Therefore it was decided to let this company develop a nozzle with dimensions fitting for the container.

This concludes the design phase for the container. The initial plan was to create a sort of elongated centrifugal pump with the impeller at its core, and I believe that this idea has been brought to fruition with this design. Below one can see what the container looks like with all its components connected.

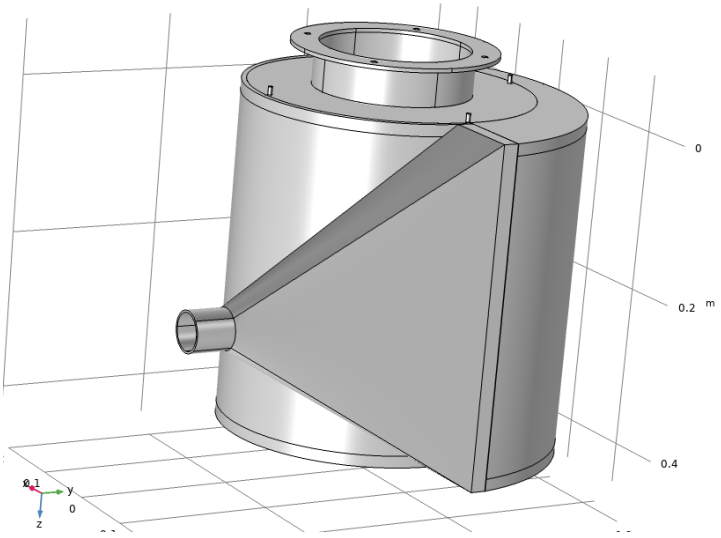

Figure 3.21: Side view of the full container design with all components attached.

All that is missing from figure 3.21 are the hoses and some simple support legs to keep it standing upright. Now it should be noted that this design is built around the fact that the container is to be built with metal. However, with this design as a baseline, one can modify it accordingly to meet the structural requirements necessary to use different materials such as plastic or wood. Without the impeller submerged, the total volume of the container (without hoses) is 60 liters.

Overall this design was not overly complicated; that is, it should not be a problem to construct and test within the allotted time of the project. The somewhat unknown parameter is, of course, the effectiveness of the impeller. Typical centrifugal pumps have very specialized impellers that are purely created to direct the flow in a specific direction. These impellers have the same radial flow pattern as the RBR, but the radial flow is naturally lessened in the RBR due to its purification components.

If the design works as intended, there should not be too much turbulent flow along the mantle wall of the container. However, the flow will probably not be fully laminar, but it should flow smoothly towards the outlet. As stated earlier, the nozzle itself will most likely become a bottleneck in the system. This fact is unfortunate but inevitable due to the circumstances regarding the available material. Besides that, if built correctly, this design of the container ought not to have any leakage issues. It should prove to be structurally intact enough to sustain the forces occurring inside during experiments.

In figure 3.22 one can see the container with all pieces split apart.

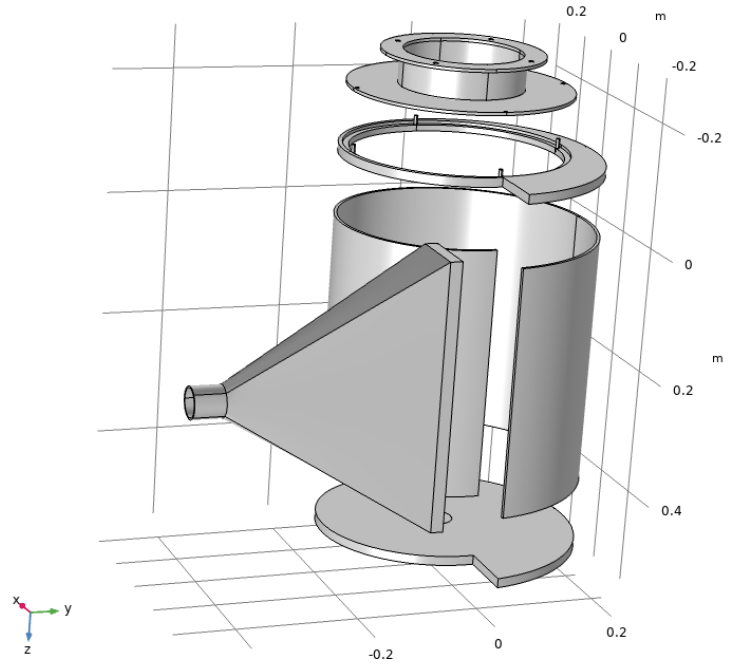

Figure 3.22: Side view of the full container design with all components split apart.

The impeller's placement inside the container will be such that the center is as close as possible to the inner wall of the spiral. This will hopefully reduce turbulent flow along the wall. A 1:1 model of the impeller was inserted into the 3D model at its prescribed location to visualize this better.

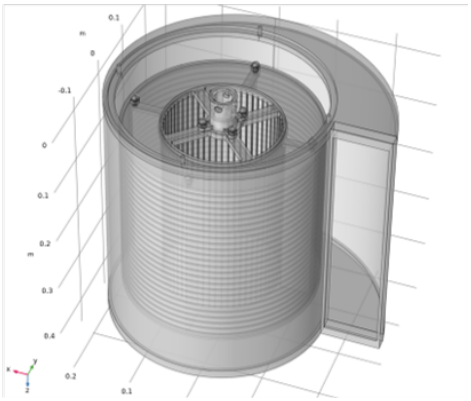

Figure 3.23: Impeller location inside the container

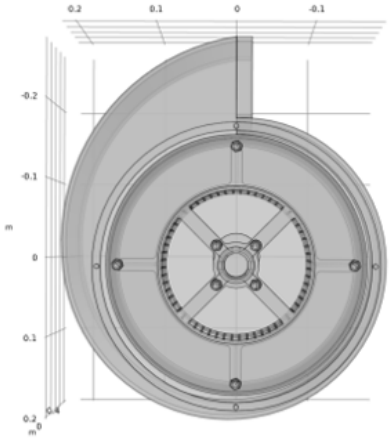

Figure 3.24: Top view of the impeller's location inside the container.

In figure 3.23 and figure 3.24 one can visualize what it will look like when the impeller is lowered into the container. Here one can see how the open area between the impeller and mantle wall increases slowly at the first half, then rapidly increases its area towards the outlet. To keep the design similar to a regular centrifugal pump, the dead space between the impeller and mantle wall is as minimal as possible while still allowing for a wide outlet.

## 3.3 *Methodology of the construction*

In this section, we will cover the entire process of the construction phase of the container. This includes planning, finding material, what tools were used, and general motivation for each step through the process. The initial plan was to let professional metal workers build the container. This would ensure that the construction would be of high quality. Any potential confusion around the design would be avoided with the CAD models, blueprints, and supervision. Constructing it in stainless steel has the apparent benefit of being a very sturdy material, i.e., it would allow for several rigorous tests at high RPM without worrying about the structural integrity. Another benefit when building it with metal is that one will have the possibility to weld all the edges. If these welds are proper, the container will be both air and watertight. Letting metal workers build it also means they can utilize the CAD models to build it nearly precisely as designed, which means the container will be very flexible during the experimental phase.

A couple of different metal workers were contacted and given the request to build the container. One metalworker was ready and willing to take up this project and estimated the price and time to construct. The price to construct the container was deemed a bit too high. As this container is only a prototype, it did not seem worth the investment. The estimated time to build it was also relatively long, and it was considered too risky to place too much trust on an external factor. For instance, if the construction hit some snag or problem and was forced to delay, we would find ourselves completely powerless in continuing the project. With these points in mind, it was decided that we take upon the task of building the container ourselves.

To build a proper container in the available time without metalworking tools such as CNC laser cutters, welding machines, and bending brakes, we decided to construct the container using wood and plastic. While these materials are not as structurally reliable as stainless steel, it is significantly easier to work with using the tools at my disposal, and I have previous experience working with these materials.

### 3.3.1 *Finding materials & planning*

The switch from metal to wood and plastic required certain changes in the design of the container. The design from the blueprints would still be utilized as much as possible, with the focus being to keep the spiral shape of the container. A big issue was that we could no longer rely on the benefit of welding. This meant that the design had to be re-done so that the container was stable and could sufficiently support the mantle wall, lids, and outlet nozzle. The major problems of the new wood and plastic design that had to be solved were as follows.

- Problem 1: Find a way to make the container both air and water-tight.
- Problem 2: Adapt the design so that it can properly support the mantle wall and other components.
- Problem 3: Make it sturdy enough to handle the forces inside, expect it to survive through tests where the impeller spins over 300RPM.
- Problem 4: Find suitable material which can withstand the water inside, i.e if wood is used, make sure its coated so that it does not start soaking up water and swell up.
- Problem 5: Find a way to construct the top lid cover, so that the new container design can be connected with the mixer motor.

Thus, the first task was to find proper material that could be utilized in constructing the container. Using the planned design as the reference over the basic shape of the container, the hunt for materials began. The most crucial bit is the mantle wall, as this needs a spiral and curved shape. It seemed natural that plastic would be a suitable material. Plastic is both smooth, rigid, and flexible to a certain extent. Having had some experience with the materialistic properties of plastic, I knew that once the plastic is molded into a particular shape, it can be quite cumbersome to form it into another shape. Therefore it was decided to start by cutting up a cylindrical barrel and using it as the mantle wall. In order to not overwhelm myself with the new design, I decided to start simple and ask the question, "How can I shape the mantle to both sit tightly and be connected to the top and bottom lid?".

Figure 3.25: View of the two basic component acquired for the construction, a plastic barrel and a sheet of veneered plywood.

The initial idea was to get two sheets of wood, use a milling drill to create a spiral-shaped indent on both sheets of wood, then insert the plastic sheet inside this indent to set it into the desired spiral shape. With this initial idea, a large veneered plywood sheet and a plastic barrel were bought. In figure 3.25 one can see the two simple components acquired to begin the construction. The veneered plywood sheet was about 12mm thick, area of 1.5m x 1.5m, and fully waterproof. As the arc length of the mantle spiral in my design was 1304mm, going by the equation determining the circumference of a circle, I needed a barrel with at least a diameter of around 410mm. The barrel I found was made out of LDPE plastic, had a height of 680mm, a diameter of 520mm, and a volume of 100 liters. It seemed like an ideal fit for the mantle wall. However, it did have a flaw. The barrel had a slight conical angle. I had searched for a perfectly cylindrical barrel but alas could not find one. However, the current barrel would suit fine as a starting point for the mantle.

Now before I started to cut and shape the materials I had acquired, I needed a physical reference of the spiral seen in figure 3.11. As the spiral starts as a logarithmic spiral with set parameters but ends with a custom circular arc at the end, I could not simply plot points from the logarithmic spiral equation to get my spiral. The idea can easily be explained with the sketch in figure 3.26

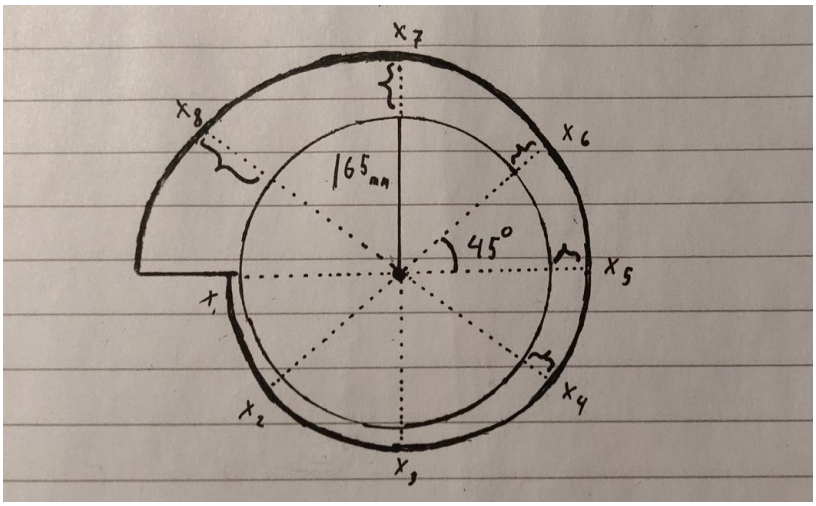


Figure 3.26: Idea over how to accurately draw the spiral in real life.

By knowing the diameter and position of the impeller inside the spiral, I can use that knowledge as a reference. Then by cross referencing the spiral in the CAD model, I can get the distance from the impeller to the mantle wall. In figure 3.26 it is split into 8 points which each depict the distance from the edge of the impeller to the wall at 45° intervals. Now, as the spiral grows in such a complex way, I settled with 180 points.

Then by using a piece of cardboard, a circular paper with the same diameter as the impeller, and the distances measured in figure 3.27, a sufficiently detailed physical interpretation of the spiral could be plotted and cut out from cardboard. This spiral can be seen in figure 3.28.

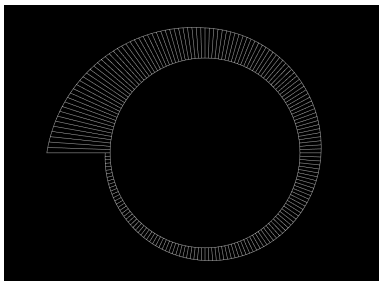

Figure 3.27: Plot of 180 distance points from the impeller to the mantle wall.

This cardboard cutout will be used as a reference for the shape of the spiral. The arc length of this spiral was almost exactly 1304mm, so it was safe to assume that it mimicked the CAD model spiral well enough. With this reference, the spiral was drawn onto the veneer plywood sheet. However, before it was time to mill a groove along the drawn spiral, I wanted to cut the barrel into a suitable mantle wall first. This was done by simply cutting the bottom and top part of the barrel. What was left was a cylindrical shell with a suitable height and diameter.

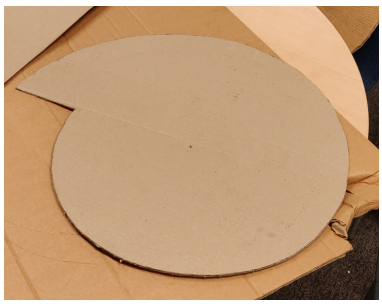

Figure 3.28: Cutout of the spiral.

In figure 3.29 one can see that the barrel does indeed take on a cylindrical shape, however, there was still a slight angle to it. The barrel started with a big diameter but slowly kept shrinking until the bottom of the barrel. The angle thus gives the barrel a very slight conical shape. Another issue was that there was a difference between the plastic thickness at the bottom and the top of the barrel. The plastic was around 1.7mm thinner at the bottom compared to the top.

Figure 3.29: The trimmed plastic barrel.

### 3.3.2 *Construction of the container*

With the plastic wall, a cutout of the spiral, and veneer plywood, the milling could begin. However, it was at this point that something became very apparent, the veneer plywood sheet was way too thin. By estimating from the rigidness of the plastic, the groove on the plywood would probably have to be 5-10mm deep on both the bottom and top sheet, and considering that the plywood was 12mm thick, I could not rely on the plywood's integrity if it became that thin at the grooves. I also realized that milling a perfect spiral groove may not be as easy as I initially assumed. So another idea was formed, that instead of milling a spiral groove on the plywood, I would cut out a spiral-shaped plywood board. This cutout would then be screwed down on a thicker wooden board. What you would have then, is a thick wooden board serving as a bedrock and a 12mm spiral-shaped plywood board screwed on top of it. The idea is to then screw the plastic wall onto the sides of the plywood spiral, thus conforming to the desired shape.

Figure 3.30: The plywood spiral cutout being screwed on a thicker wooden board.

In figure 3.30 one can see what is essentially the base of the container. The bottom wooden board had a thickness of 40mm.

Now for the top part of the container, the same thing was done but inverted. The plan was to use a thick wooden board of sufficient size, cut out the spiral with the help of a jigsaw, and then use the hollowed-out frame. It would look something like this.

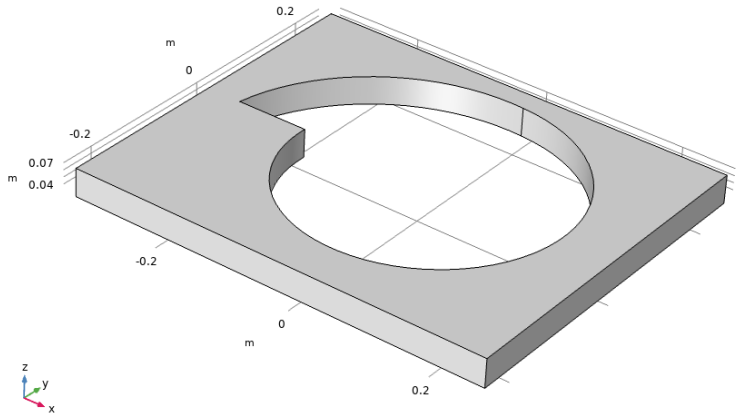


Figure 3.31: Simple model of the renewed design for the top part of the container.

The idea of the design in figure 3.31 was thus for this frame to be lowered down onto the plastic wall, and then the wall would be screwed onto the sides of the frame. One can see the process of cutting out the spiral in figure 3.32. Thus the spiral mantle would be screwed both to the bottom plywood spiral cutout and along the wall of this spiral wooden frame, ensuring that the wall is nicely settled into its desired shape. Now with the main components built, it was time to try building it up together.

Figure 3.32: The frame used for the top of the container in the process of being cut out with a jig saw.

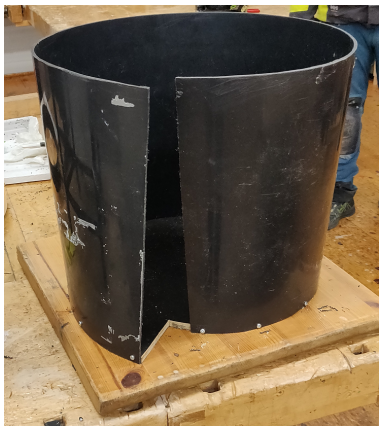

Figure 3.33: Attempt of getting the cut up barrel to fit as a mantle wall for the container.

When the trimmed plastic barrel was fitted alongside the veneer plywood spiral sheet at the bottom, it became quickly apparent that the angle observed earlier was indeed a lot steeper than initially expected. The leaning angle together with the fact that the diameter of the barrel is gradually shortened from top to bottom had the consequence that it would not perfectly conform to the spiral shape. In figure 3.33 the effect of the internal, conical angle of the barrel becomes easily visible. While the top part has enough arc length to cover the entire surface, the bottom part was shy 30mm to reach the end. While this might be fixed through cumbersome stretching and adjusting of the plastic, it was deemed that the barrel simply be thrown away and look for another alternative. While the cylindrical shape of the barrel allowed it to shift into the spiral shape flexibly, it was not easy to find perfectly cylindrical barrels that met the needed dimensional requirements.

Therefore it was decided to simply buy a plastic sheet and utilize the tools to my disposal to form it accordingly. A sheet of clear, 3mm thick polycarbonate plastic was found. It was cut with a length of around 1400mm and a height of 400mm. Why it was a longer length than the specified spiral arc length will be elaborated on soon.

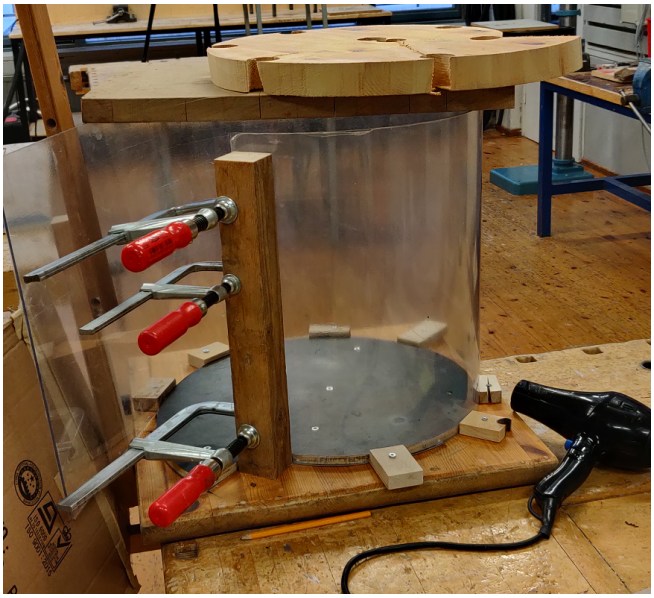

Figure 3.34: Forcing the plastic sheet to the desired spiral shape.

One can see the efforts needed to force the straight plastic sheet into the spiral in figure 3.34. The blocks and C-clamps did an excellent job of keeping it in place. However, when using plastics one can with the help of heat form it into other shapes. With the spiral steady, it was heated along the edges. Firstly a regular blow dryer was used. However, its heat output did not have much effect on the plastic. Therefore it was replaced with an electronic heat gun.

The heat gun seen in figure 3.35 was used to gradually warm up the plastic sheet, especially at the start of the spiral, where the forces were the largest. As the heat gun provides significantly more heat than the blow dryer, it was made sure to be extra careful not to cause the plastic to melt. After heat treating the plastic, the sheet was now much easier to bend into the desired spiral shape. With the sheet now taking on a shape that can be easier to work with, it was time to fasten it to the bottom of the container.


Figure 3.35: Using an electronic heat gun to warm up the mantle wall.

One big problem when working with plastic and wood in this construction is that there is a high chance of leakage. Simply screwing the plastic mantle to the veneer plywood and top frame would most likely not be enough to seal it and prevent it from leaking. If the container had been built with metal, welding would have been used to both seal and connect the components of the container. So something was needed that would work as a substitute to a welding seal, but for wood and plastic. A perfect candidate for this would be mounting glue. This adhesive material will form a strong bond between the materials and fill up any gaps easily. The strength of the adhesive used had a holding strength of up to 5 kiloNewtons. For all intents and purposes, this material was an absolute lifesaver in this project. Without it, the structural integrity of the container would have been significantly worsened. As the plastic mantle was fastened onto the veneer plywood, this mounting glue was applied to the side of the plywood where it would form an extra adhesive and seal.


Figure 3.36: Fastening the mantle to the veneer plywood sheet.

In figure 3.36 and 3.37 one can the process of fastening the plastic mantle to the bottom veneer plywood sheet. If one has worked with plywood sheets before, one ought to realize a flaw in the way the plastic mantle is fastened with the plywood in figure 3.36, mainly the direction of the screws. As plywood consists of several small wooden planes stacked on top of each other in layers, one generally wants to screw through these layers, not alongside them. However, in this case we had no other choice, so to compensate for this, mounting glue was used along the edges to strengthen the hold. In order to increase the structural integrity of the mantle wall and container, several wooden support beams were also placed alongside the mantle wall. These beams were then connected to the wooden bottom board with long screws.

Figure 3.37: Alternative angle, here one can also see the support blocks along the sides.

With the mantle connected to the base, the next component to create was the outlet frame. The basic design was to use the one in figure 3.19 with the blueprint 37. The only modification to this design was to make the left and right sides of the frame thicker. The motivation for this was that was I no longer can weld the outlet nozzle to the frame. I need some added space where I can fasten the nozzle to the frame with screws. The outlet frame was created using 20mm thick veneered plywood.

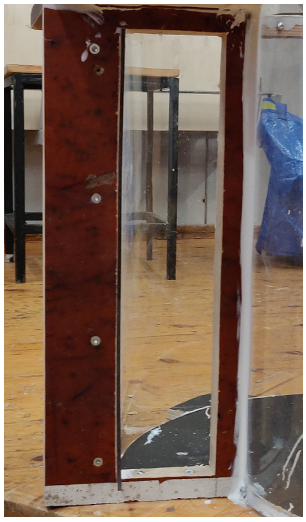

Figure 3.38: Outlet frame created out of veneered plywood.

As seen in figure 3.38, the left and right sides of the frame are thicker, especially the left side from this point of view. The motivation for keeping the left side so much wider is that there is a wooden support beam behind it, so the screws visible in the figure connect the frame to that support beam. This wooden beam is also fundamental, as it makes extra sure that the outlet portion of the spiral does not move about, as it will otherwise try to return to its original shape.

In figure 3.39 one can get a better view of how the entire thing is supported. The small blocks along the bottom of the mantle, together with the wooden support beams, help force the plastic sheet into its shape. One can also notice that the plastic mantle is sticking out a bit from the outlet frame here. As mentioned earlier, the plastic sheet had a length of around 1400mm, i.e., almost 100mm longer than the arc length of the designed spiral. The motivation for this was to create a more smooth transition between the container and the outlet nozzle.

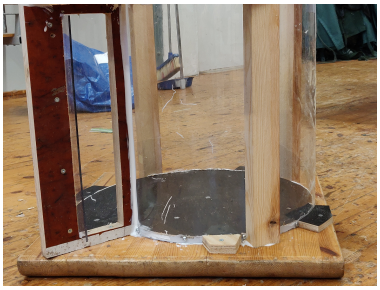

Figure 3.39: Outlet frame, plastic spiral mantle and wooden support beams.

Next up was the top frame. As a new mantle wall was acquired, a new top frame was made to fit more properly. Another top frame was built using a 20mm thick sheet of veneered plywood utilizing the same idea as earlier.

In figure 3.40 one can see how the top frame is holding everything firmly together. With this design, the forces of the plastic mantle trying to go back to its original shape ought to be evenly distributed along the base, top frame, and support beams. Here it is also visible that the top frame was also fastened together to the support beams. A nice layer of mounting glue was placed between the mantle wall and top frame, as well as covering the support beam screws, preventing them from rusting or causing the plywood to soak in water.

In figure 3.41 one can see how the top of the mantle wall was fastened to the frame. During this process, it was naturally made sure to be careful with the torque on the screwdriver. Allowing too much would probably cause the plastic wall to crack, which would inevitably cause leaking. In figure 3.42 one can see how the mantle is fastened along the side of the outlet frame. This was done since that spot was the most challenging part to bend, so extra support was necessary to keep it in place.

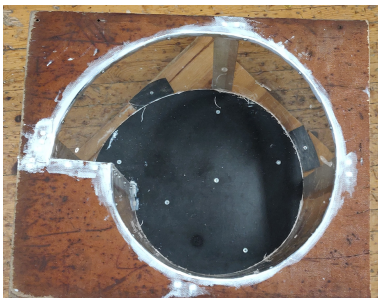

Figure 3.40: New top frame created for the container.

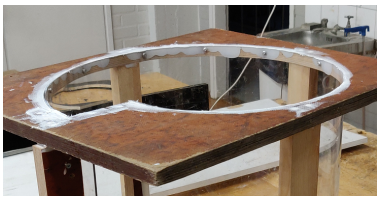

Figure 3.41: Fastening of the mantle to the top frame.

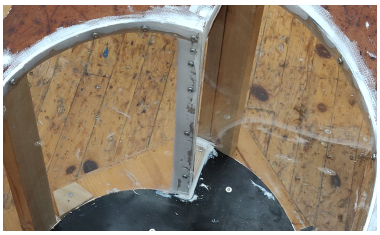

Figure 3.42: Alternative view.

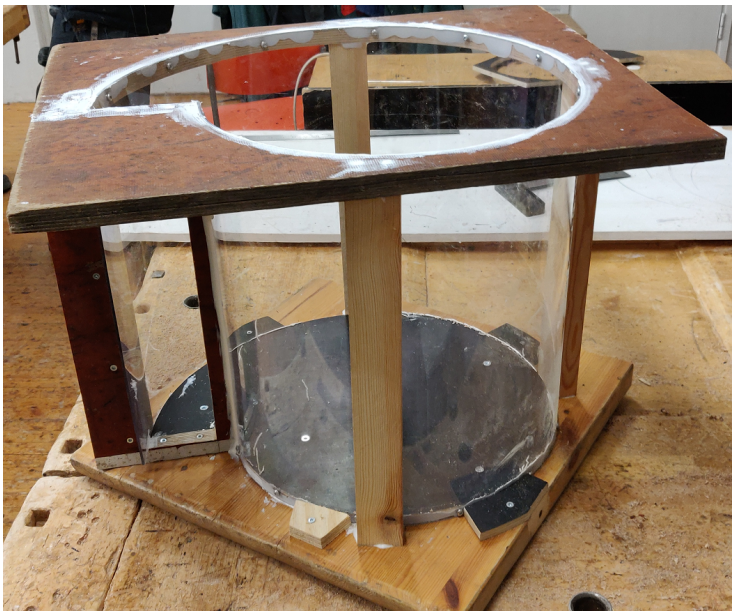

Figure 3.43: Frontal view of the container progress thus far.

With the top frame fastened, the container was now almost entirely built, as seen in figure 3.43. The only things missing were the top lid cover, outlet nozzle, and inlet. Here one can also appreciate the fact that the plastic mantle is transparent, unlike the previous plastic barrel. The obvious benefit of this is that with a transparent wall, one can easily witness what is going on inside the container during experiments. It will be possible to spot turbulent behaviors and if cavitation bubbles occur during tests with high RPM.

At this point, with the outlet frame built, an order request was sent to a manufacturer to start constructing the custom-made nozzle. While waiting for that component to arrive, plans were made to figure out how to make the inlet. The wooden board plus the spiral veneer plywood sheet had a combined thickness of around 50mm, which meant the inlet would have to go through all that and still stick out enough from the bottom to allow for a hose to be connected. The initial idea was to utilize a threaded hose nipple that could be screwed onto the bottom of the container.


Figure 3.44: Initial idea for the inlet.

The inlet in figure 3.44 consists of a 50mm long internally threaded cylinder and a threaded hose nipple with a 2" diameter. While this would probably work as the inlet, the problem would be finding a way of fastening the grey cylinder to the container. While definitely possible, it was deemed to be too cumbersome. I came upon a component utilized in boats called a *through hull fitting*. These components have exactly the shape which I was looking for in my inlet.


Figure 3.45: Through hull fitting used for boats.

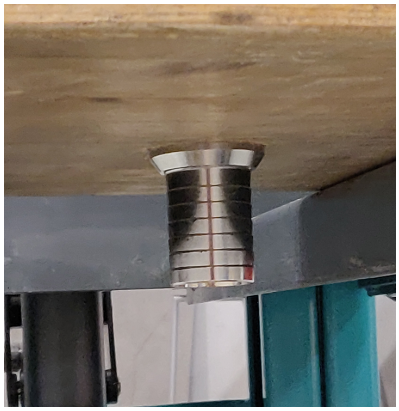
Figure 3.46: View of the inlet from the bottom of the container.

The through-hull fitting found in figure 3.45 was around 100mm long, had a flange with three fittings, and a hose nipple with a 1.5" diameter. So overall, it was a perfect fit for an inlet. The only issue is the fact that it was a bit more narrow than I wanted, but using a 1.5" hose should not be a problem. With the inlet acquired, it was time to install it. Now the important part was to make sure that the inlet was positioned directly below the center of the impeller in order to prevent the flow from the inlet from becoming too turbulent. In order to do this, the impeller was lowered into the container, positioned at the desired location. Then a marking was set on the bottom plywood sheet directly below the center of the impeller. With the marking set, the hole could be cut out with a hole saw. As seen in figure 3.46 the inlet sticks out perfectly from the bottom of the container, allowing a hose to be connected to the inlet easily.

Next up was trying to solve the problem of the top cover. As I could no longer utilize the top cover design proposed in 3.21, I would have to find another way of sealing the container and also connect it to the mixer motor. First and foremost, in order to prevent water from leaking from the top, a gasket was put around the spiral of the top frame. This can be seen below in figure 3.47

Figure 3.47: Figure showing the position of the impeller inside the container, as well as the gasket created along the spiral on the top frame.

The idea with this gasket was to simply place a veneer plywood sheet with a hole for the motor shaft on top of the top lid, and then the gasket would create a seal. This veneer sheet would be the equivalent to the top lid in my earlier design, meaning that I still needed a top lid cover to seal the container fully. My initial idea was something akin to creating the cover seen in figure 3.17 using wood. Nevertheless, I quickly realized that why not simply use the top lid cover that already exists on the mixer motor. Using this cover, I can both save much time and assure myself that this component is appropriately compatible with the mixer motor. Now, as this cover was made for a different container, certain adjustments had to be made so that it would be compatible with this new design.

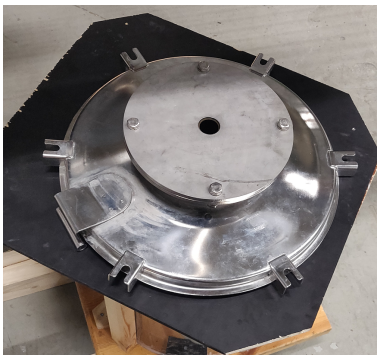

Figure 3.48: The top lid (black plywood veneer sheet) and cover together.

The basic idea for the solution of the top lid can be visualized here in figure 3.48. While the top lid cover looks quite compatible from this point of view, it did have some problems. The main issue was the lip which protrudes at one spot. It can be seen at the bottom left of figure 3.48. This lip was used as an added locking mechanism on its intended container. The lip caused the cover to be lifted upwards, so it was cut off using a metal saw. The second issue was finding suitable locations to fasten the cover to the container itself. As one can see in figure 3.48, the top lid cover has six arms where one could put bolts through and connect it to the container. By removing the veneer plywood sheet, one can more easily visualize this problem.

Figure 3.49: The top lid cover placed on the container without the top lid.

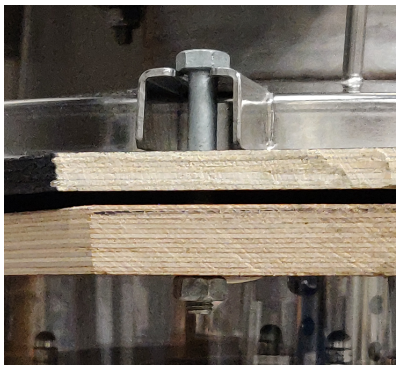

Figure 3.50: Bolt connecting the top lid cover with the container.

Here in figure 3.49 it becomes apparent that there are many locations on the cover arms where bolts simply cannot go through the top lid frame, as it would either hit the gasket or be inside the container. However, it was found that at two diagonal places, bolts could go through the cover arm, top lid, and top frame, and at one place where it could go through at least the top lid cover. Holes were drilled at these locations and fitted with long enough bolts and nuts to tighten them up, as can be seen in figure 3.50. This, together with the top lid cover pressing down on the top lid, which in turn will be pressing down on the gasket and top lid frame, resulted in a suitable seal for the container.

At this point, the ordered outlet nozzle had arrived at the workshop. It had the exact dimensions as requested and thus fit perfectly. All that needed to be done was to drill a couple of holes along its flange so one could screw it into place. Naturally, the area between the flange and outlet frame was covered with a layer of mounting glue to prevent leakage.

With the outlet nozzle seen in figure 3.51 fastened, the container was now as good as finished! Comparing the finalized container to the one in my initial design shows that quite many changes had to be made for the container to work with the new materials properly.

Figure 3.51: The custom made outlet nozzle.

This final design was probably much more optimal, as one must remember that the container is merely a prototype. If this design does show promise, it could be built from stainless steel using the developed blueprints. However, for conducting the planned tests, this container ought to do just fine. Legs were added to the bottom so that a hose could more easily be connected to the inlet of the container and keep it upright and level.

Figure 3.52: The final constructed design of the container.

The finalized constructed design can be seen in figure 3.52, the main goal was to get the mantle wall as similar to the proposed spiral design as possible. With the modifications to the design, the mantle wall had an excellent spiral shape akin to the one initially proposed. The only discrepancy is at the outlet. As the frame had to be a bit thicker than initially planned, it leads to a straight surface that might cause some resistance in the flow. If this proves to be the case, one can add a component known as a cutwater. This is simply an angled piece that will prevent the flow from crashing into the straight wall and instead flow directly to the outlet. This concludes the construction phase of the container.

## 3.4 *Methodology of the CFD simulation*

This section involves the development of the computational fluid dynamics (CFD) simulations during the project. The motivation of doing these simulations is mainly to get a clearer idea of the flow inside the container and figure out which components have the highest impact on the flow rate of the water. These simulations will also be able to provide much information regarding the forces occurring inside the container. One can easily visualize the velocities and pressures involved. The software used to create these simulations was COMSOL Multiphysics (version 5.5). All results recorded from these CFD simulations can be found in the results section of this paper.

For the simulation to properly depict the real-life experiment, it needed to employ the correct physics and boundary conditions. So for starters, a suitable physics model for the flowing water needed to be found. As the models and shapes had been designed earlier, I could only focus on understanding how the CFD tools and physics worked within the software. I decided to start simple, seeing if I could create a spinning impeller in 2D and get it to displace water. It should be noted that the sections in this entire methodology did not occur in chronological order, i.e., the simulations were developed alongside the design and construction phase. Due to this, one can notice how some of the models used in the simulation experiments are quite outdated compared to the final designs. The first simulation utilized a laminar flow model in a 2D environment replicating a cross-section of the container.

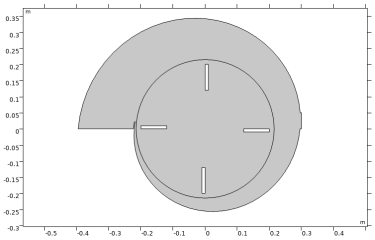

Figure 3.53: 2D model depicting a cross-section of the container.

In figure 3.53, one can see the first simple 2D model for simulation. The inner-circle represents the *rotating domain* of the simulation, i.e., this is the domain depicting the spin of the impeller, which can be seen here as four rectangular pieces or wings, if you will. These wings will rotate in a counter-clockwise direction at 120RPM. The outlet was placed at the end of the spiral, and the inlet is the little indent on the right. The boundary conditions at the inlet were a low 0.1m/s inlet velocity, and the boundary condition for the outlet was a condition dependent on the pressure. Figure 3.54 depicts the mesh of the model; it is on all of these small triangles, known as cells, where the fluid dynamics calculations will be done. In this test, a rather fine mesh was chosen. The simulation was done on a time-dependent study, meaning that the simulation results can be plotted on different time steps. This simulation depicted an 8-second run, where every 0.5 seconds was plotted out.

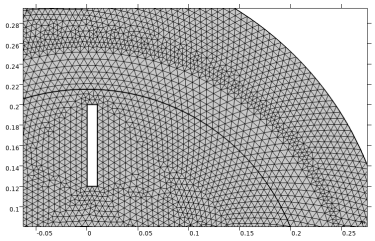

Figure 3.54: Mesh for the first model.

As the flow occurring within the container in this project will most likely exhibit turbulent properties, one cannot rely on a simple laminar flow model. Due to this, a model that considers this turbulent behavior was chosen instead. Several different models can handle turbulent motions, but the one chosen in this project was the Tur-

bulence model $k-\omega$, as it was beneficial for simulations where the fluid had to go through curvatures. The same 8-second simulation was conducted with the Turbulence $k-\omega$ model.

After getting confident enough with the 2D simulations, it was time to step it up into 3D. This would significantly increase the complexity of the CFD simulations, and therefore it would become more difficult for the solution to converge. Therefore it was decided to start off as simple as possible. If the simple simulations converged and gave reasonable results, they would continuously be made more complex until they replicated the real-world experiment as closely as possible.

Thus a fitting, simple 3D model of the container was developed. The main idea was to keep it as simple as possible by only modelling the spiral container. As the actual impeller is a very complex structure, it was decided to simplify it to its most essential components. Therefore as in the earlier 2D simulations, it would only depict the four impeller wings, which can also be seen in figure 1.5. The following 3D simulation model was made. Do note that this model used the unoptimized spiral shape from figure 3.6.

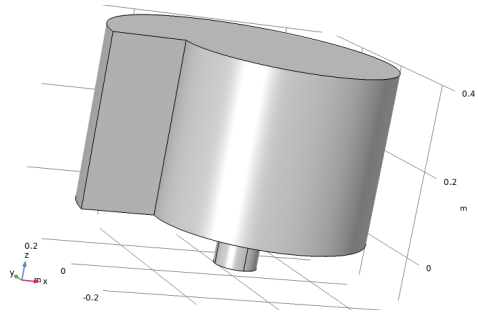


Figure 3.55: 3D model of the spiral container.

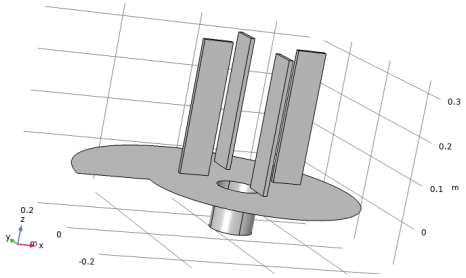


Figure 3.56: Interior of the spiral container, showing the impeller and inlet.

One can see the simple 3D model for the simulation at figure 3.55 and figure 3.56. The boundary conditions for the outlet and inlet were the same as in the 2D simulation, i.e., a velocity at the inlet and pressure at the outlet. However, a few things were simplified in order to help the simulation reach convergence. First and foremost, the model was no longer a time-dependent study. The reason for this was the fact that getting a 3D CFD simulation to work properly with a time-dependent study was quite a big challenge at this point. So an alternative study was chosen, the frozen rotor study. This study is a special case of a stationary study, i.e., it is not dependent on time. With this study, as the name suggests, the rotor is frozen in position, and the subsequent rotation of the domain is accounted for by including Coriolis and centrifugal forces. While more simplistic than the time-dependent study, this study is well suited for acquiring a good estimate of the flow inside the container. At first, it was quite troublesome to get the simulation to converge, but setting a pressure point constraint somewhere on the model fixed this error.

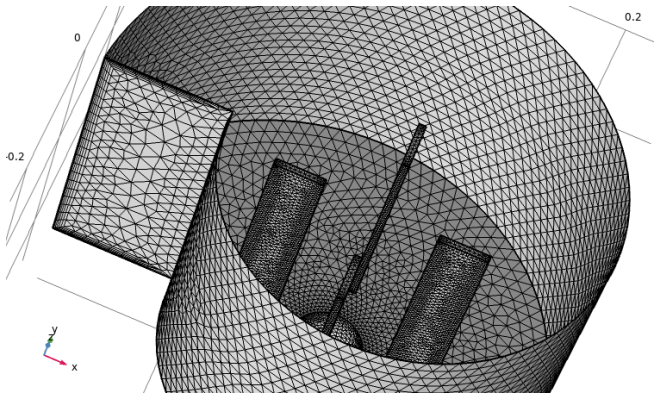


Figure 3.57: The mesh of the initial 3D simulation.

In figure 3.57 one can see the mesh utilized for this model. When it comes to CFD model meshing, one can spend a very long time optimizing the mesh to be perfect for the experiment. The basic idea of creating a fitting and good mesh when it comes to CFD simulations is to have a fine mesh at areas where the flow is very chaotic and turbulent and keep the mesh coarser at areas where the flow will be calmer and more laminar. After spending quite some time experimenting with different ways to optimize the meshes, with no good results, it was decided to leave it to the automatic mesh creator in the software to handle it in order to save time.

It was at around this point where I made the decision to tighten the spiral at the outlet, so that the amount of dead space between the impeller and the container mantle was as little as possible.

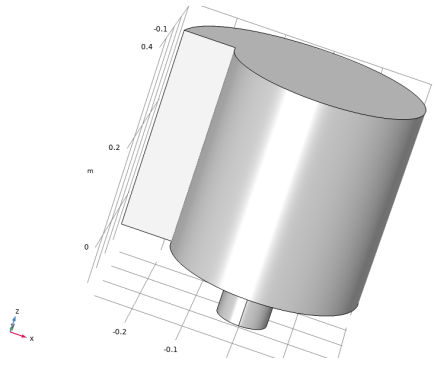


Figure 3.58: 3D model of the optimized spiral container.

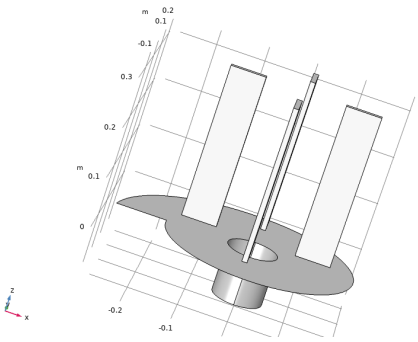


Figure 3.59: Interior of the optimized spiral container, showing the impeller and inlet.

As the geometry was smaller in the model used in figure 3.58 and 3.59, the mesh size was set to coarse to keep complexity at a manageable level.

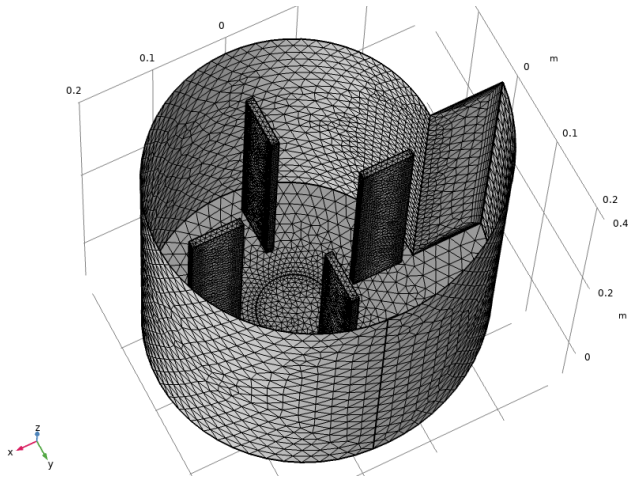

Figure 3.60: The mesh of the optimized spiral 3D simulation.

The mesh created in figure 3.60 is relatively coarse at the walls, which should fine as the flow here is not so violent but still pretty fine at the impeller wings, where most turbulence will occur. This model was tested several times at varying rotational velocities. The computational time for each was at around 5 hours.

At this point in the simulation phase, I tried my absolute best to get a time-dependent study to work. One issue with time-dependent studies of this scale is that they are quite sensitive to the initial values. Thus I started by first doing a frozen rotor stationary study at some set RPM and then using the results from this study as the initial values for my time-dependent study. With the initial values set, the rotating domain had to be modified to work with the time-dependent study properly. To do this, something called a sliding mesh was made. This method gives the most accuracy when simulating flows in a multiple moving reference frame, but at the cost of more computational power. Attempts to get this method to work were made by creating sections of the rotating domain (the impeller) and defining these domains into an identity pair. This identity pair was then used together with a flow continuity condition, which allows the flow field to be continuous in this area. However, after several days of painstakingly trying to get this time-dependent study to work, it just kept crashing. Thus it was decided to keep conducting simulations with a frozen rotor study, as the results from these were considered sufficiently close to reality.

So now, with the 3D model working at high RPM using the frozen rotor study, it was time to start making it more and more like the real-life experiment. First and foremost, the nozzle was added. This was not difficult as the nozzle had already been designed, so it was just imported and put into position. One problem I had with the earlier model was the uncertainty of picking the correct boundary conditions for the inlet and outlet. Especially the condition at the inlet did not seem quite correct, that is, just having a fluid velocity.

However, as my actual experiment will only be testing the capabilities of the container itself, i.e., a hose will go from the outlet loop around and get connected into the inlet, I realized something. Why don't I simply do the same thing for my CFD model? That is, I remove the boundary conditions for the inlet and outlet, create a fitting hose that connects the container to itself, and then just let the physics of the CFD do the rest. Using this idea, the following CFD model was made.

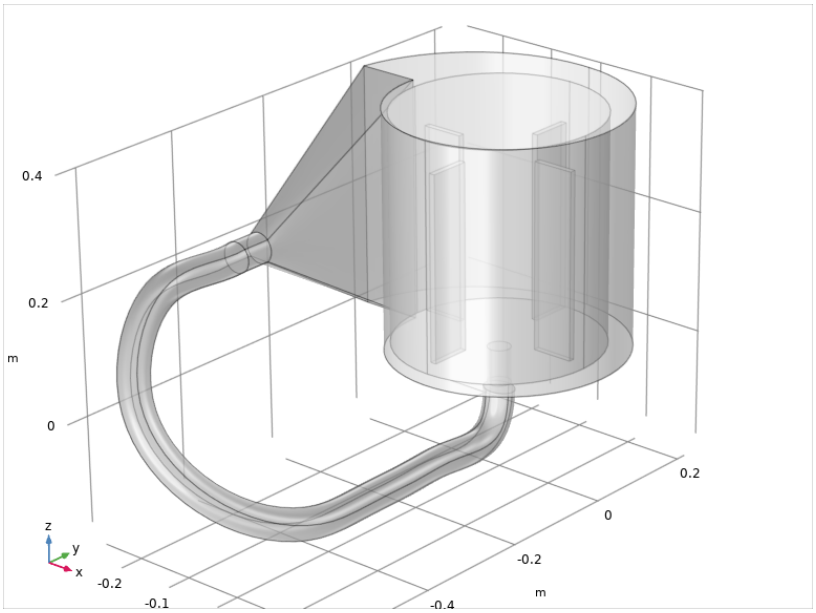


Figure 3.61: The new CFD model where the container is connected to itself with a hose.

In figure 3.61 one can see a transparent view of the new model. By being connected to itself in a closed-loop, no boundary condition for the inlet or outlet was necessary. The hose was created by first making an interpolation curve that started at the outlet and moved towards the inlet, then doing a sweep on this curve to get get it to the proper 2" diameter. As the inlet of the actual container was a 1.5" nozzle, the hose shrinks at this location to properly fit. Several tests with varying RPM were tested using this model.

Yet again, the mesh setting for this model was kept coarse, as any higher would utilize more RAM than I had available. The mesh can be seen in figure 3.62 and 3.63. Naturally, the mesh could be optimized to prevent this, but due to time restrictions, this could not be done. As this model worked well and did converge without any issue, the detail was increased to depict the real experiment further. The first thing to change was the hosing. In the real experiment, the hosing was a bit longer and segmented into two different hoses, a 2" diameter hose and a 1.5" diameter hose. The real experiment started with a 1 meter long 2" hose from the outlet to the flow sensor. After the flow sensor, it leads into the 1.5" hose, which goes for about 1.5 meters into the inlet of the container.

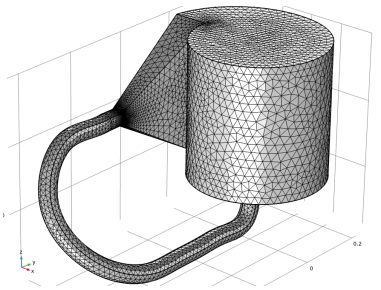

Figure 3.62: Mesh of the container with hose.

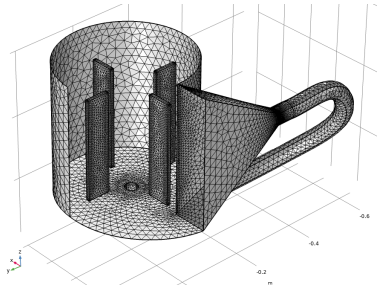

Figure 3.63: Interior mesh of the container.

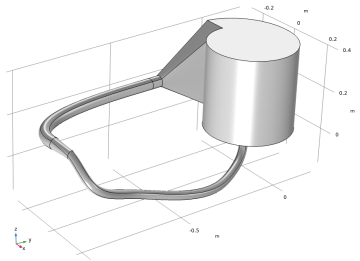

Figure 3.64: CFD model with hoses that represent the experimental setup.

At this point, the actual container and hosing were done to more closely depict the real scenario, as can be seen in figure 3.64, however, the issue of the impeller remained. The impeller was arguably the most important component in actually getting correct results, but its high detail made it fairly difficult to model. As small geometries require small cells and meshes, it will cause the needed computational power to increase by a lot. So while it would have been nice to utilize a 1:1 model of figure 1.4 as the impeller in the CFD simulation, but a compromise would need to be made. In the actual impeller, there are quite a lot of details blocking the main four impeller wings. Firstly there is an outer shell composed of a cage structure. It is this cage that contains the packed bed of ion-exchange resin or similar material which is responsible for purifying the fluid. This cage consists of 27 rings with a thickness of 2mm, starting from the bottom and going to the top with 10mm between each ring. Between each ring is a sift-type structure to allow water to pass, but not the resin material. This outer cage can be visible in figure 1.4. The four impeller wings have a width of 50mm, a height of 300mm, and a thickness of 3mm. On the inner side of the impeller, the same sift-type structure exists but is held together with 60 thin rods covering the inner wall in a circular pattern. These rods have a thickness of 2mm and a height of 300mm. The distance between each rod is about 10mm. With this knowledge, one can see that the 1:1 geometry of the impeller is very small and detailed. Creating a mesh for such an object would have to be very fine and require a lot of computational power if one wanted to run simulations on it. Making some compromises, the following impeller was modeled.

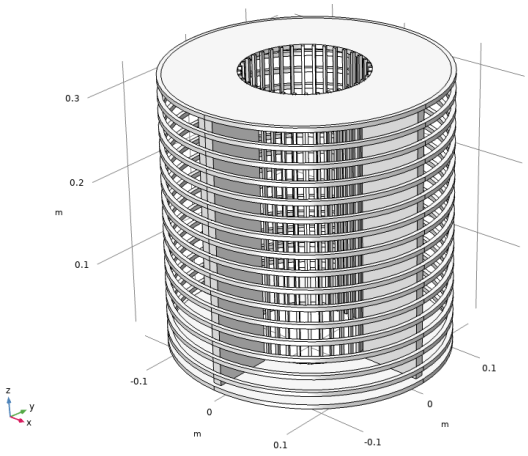


Figure 3.65: Outside structure of new impeller.

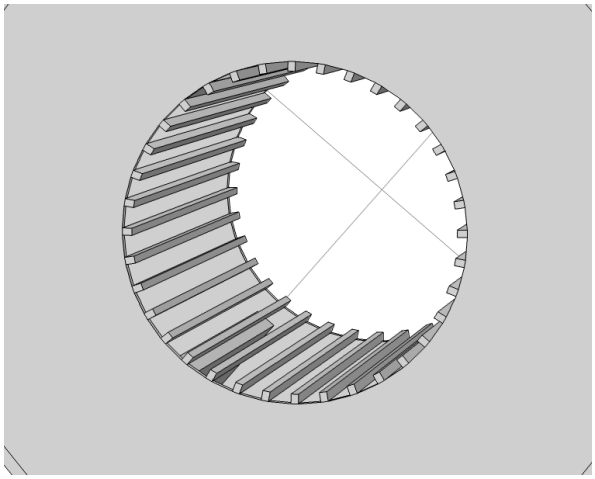

Figure 3.66: Inside structure of impeller.

While the impeller in figure 3.65 and figure 3.66 is not perfectly equivalent to the schematics of the real one, it should at least behave closer to reality compared to the previous iterations. In this model, the rings and rods are fewer than in reality but compensate

for this by being thicker. The added geometries will indubitably cause added resistance to the flow, lowering the overall fluid velocity. The geometry still contained a fair bit of small details; this caused some problems when trying to create the mesh, especially when creating the boundary layer mesh. This type of mesh has a dense cell element distribution and is most often used in fluid flow problems to resolve thin boundary layers along the no-slip boundaries (the no-slip condition assumes that the fluid will have zero velocity relative to a solid boundary). The mesh was therefore made extra course at the impeller.

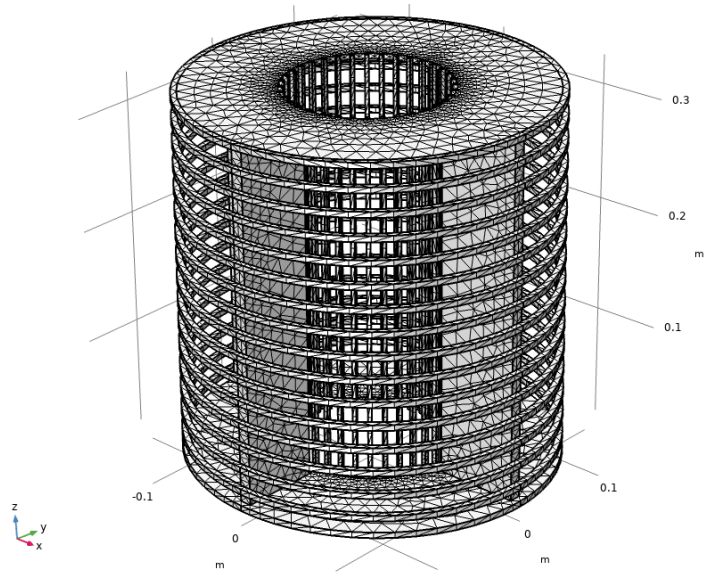


Figure 3.67: The mesh for the new impeller.

The mesh in 3.67 was built without any errors, so it was deemed good enough to be used for the simulations. An attempt was made to make the mesh even finer, but running a simulation caused the computer to run out of available RAM.

With the more detailed impeller done, the final model for the simulation was completed. The majority of the CFD simulations were conducted on this model, using the same parameters as those in the real life experiments. One notable discrepancy, however, is the flow sensor. In reality, this sensor consists of a set of fins that calculate the flow depending on how fast they spin. In this model, these fins are not present, and the water can flow through the hose unimpeded.

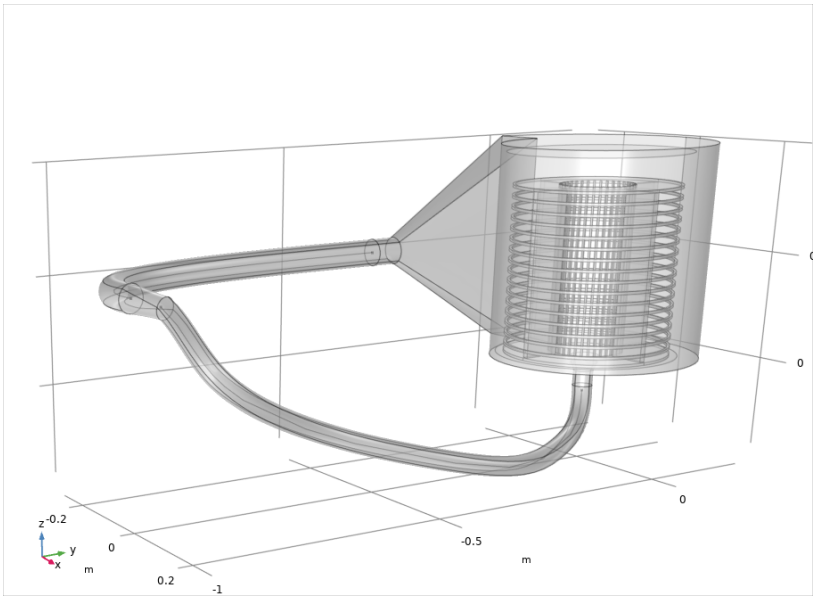

Figure 3.68: Transparent view showing the final version of the CFD model.

With this model in figure 3.68, accurate results ought to be collected from the tests, which can be compared to the results from the real-life experiments. These results will hopefully shed some light on potential flaws in the design. The simulations conducted on this model usually had no significant issues in converging. However, occasionally the simulation would get caught in a loop where the convergence leveled out and never reached a point to print out results. This was most likely due to the geometry's added complexity, which caused the simulation to be even more sensitive. These problems were solved by simply rebuilding the mesh and restarting the simulation.

## 3.5 *Setting up the experiment and testing*

This section consists of showing how the experimental setup of the project was built up. At first, the plan was to do something akin to figure 1.3, but as the goal was to only focus on the performance of the actual container, it was decided to simplify it.

### 3.5.1 *Experimental setup*

Therefore the plan was to connect the container with itself in a closed loop using suitable hoses. Firstly a 2" hose was connected to the outlet. There was some problem with this as the dimensions of the outlet nozzle had a diameter slightly bigger than 2", so the hose would simply not fit at first. But, by trimming the hose and applying grease, the hose fit perfectly on the outlet nozzle.


Figure 3.69: The 2" hose connected to the outlet nozzle.

As the outlet nozzle did not have specific grooving as most nozzles do, there was the issue of finding a way to prevent the backflow of water. A solution was simply to add a lot of mounting glue around the hose to prevent it from leaking at the outlet. Mounting glue was also applied to the welding seams along the outlet as they did not seem to be perfectly tight.

Next up was to connect the flow sensor to the pipe. This sensor would be the primary way of analyzing the flow rate of the container. The sensor had two parts, a digital display, and a sensing element. Inside the sensing element were a couple of fans that would start spinning as the fluid passes through them. With this information, the computer inside the sensor calculates the flow rate in liters per minute. The sensing element of the flow sensor had a diameter of 2", which meant it fit perfectly to the hose on the outlet, however as the hose leading up to the inlet would have to have a diameter of 1.5", it meant that a way to properly go from the 2" sensor to the 1.5" hose had to be devised. This was not a very big issue as there exists a lot of piping connectors for this exact purpose. A bridge connector between the sensor and the 1.5" pipe was thus created, as can be seen below.

In figure 3.70 one can see the transition between the two hoses, going between the sensing element. Any threaded areas on this connector were covered with thread tape to prevent leakage. Now with the hoses connected, it was time to put the impeller into position and connect it with the shaft.

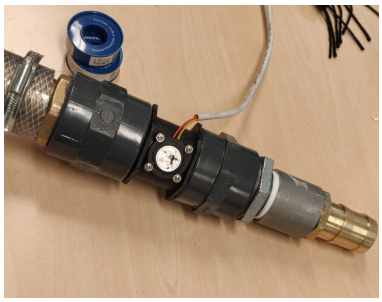
Figure 3.70: The module containing the sensor connecting the 2" hose to the 1.5" hose.

As this shaft was the factor setting the entire impeller into rotation, this step needed to be done correctly to avoid any potential accidents. One would not want the shaft or impeller to come loose when spinning nearly five rotations per second. The starting position of the shaft was a bit too far down, so a measurement was made to see how much the shaft needed to be adjusted. After the adjustment, the impeller was fastened tightly together with the shaft with the help of a threaded bolt, as can be seen in figure 3.71. With this adjustment, the impeller would be around 10mm above the bottom of the container when fully submerged.

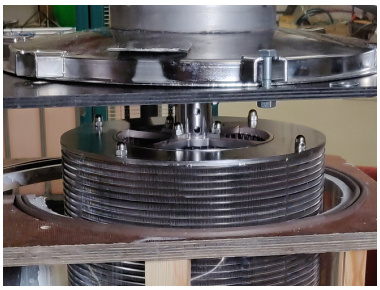

Figure 3.71: Adjusted shaft and connected impeller.

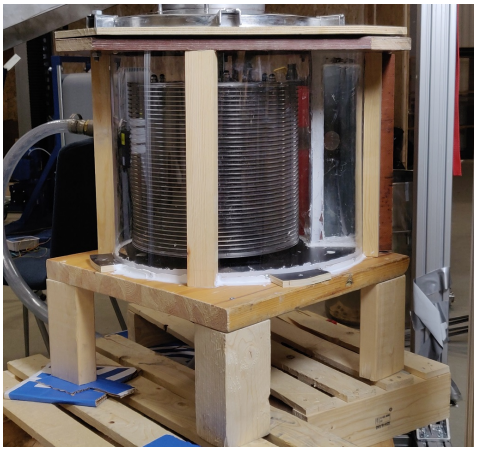

Figure 3.72: Back view.

Figure 3.73: Front view.

In figure 3.72 and 3.73 one can see the dry experimental setup with the container submerged. Thus, the shaft goes from the top lid cover through the top lid veneer sheet, and then the impeller is fastened to it. The inlet is directly below the center of the impeller. A potential issue here was the hole drilled on the top lid to allow for the shaft, as water may get through it during tests with high RPM. Otherwise, one can see that the top lid is pressed down nicely onto the container, creating a good seal with the spiral gasket seen in figure 3.47. With everything set up, it was time to start conducting the flow rate experiments.

### 3.5.2 *Flow rate testing*

The container was slowly filled with water up to a specific point so that with the impeller fully submerged; it would not cause the water to leak over the edges. With the container filled up with the right amount of water, the lids were fastened tightly. At this point, the container was inspected for potential leaks. Thankfully no air bubbles could be seen forming inside the container, and no dripping along the pipes either. The mounting glue had done an excellent job as the container was completely watertight. Next up was to check the mixer motor settings.

In figure 3.74 one can see the two dials controlling the mixer motor. The left dial sets the direction of the flow, L is counter-clockwise, and R is clockwise. The right dial goes from 0-10 with increments of 0.5, and it controls the rotational velocity. It was known that the fastest RPM was at 320RPM. However, in order to be extra sure of the RPM at each 0.5 increments, a tachometer was utilized.

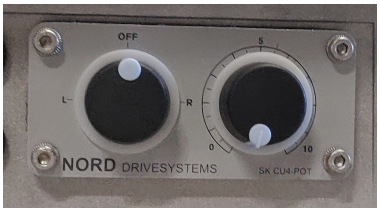

Figure 3.74: The dials on the mixer motor.

In order to properly get the tachometer in figure 3.75 to read the correct RPM, a sheet of non-reflective paper was placed around the shaft. On a small segment of this shaft, a reflective tape was placed. Now by shining the laser onto this area, the light would reflect back to the light sensor every time it passed the reflective surface; by counting the number of times this sensor is triggered in a given time frame, the RPM of the shaft can be calculated and displayed.


Figure 3.75: The tachometer utilized to analyze the RPM of the mixer motor.

The first trial started with the impeller going in the counter-clockwise direction. The dial was moved up in 0.5 increments. On each increment, the tachometer was used to get the RPM, and three readings from the flow sensor were recorded. During the first trial, this was done up until 160RPM. At this point, the container started leaking at the top lid cover. This was because the water started getting inside the hole for the shaft at the black veneer sheet.

In figure 3.76 one can see leakage caused by the faulty seal at the top lid cover. Before one could proceed to test the container at even higher RPM, this issue had to be fixed. The solution was to create another gasket that fit the top lid cover.

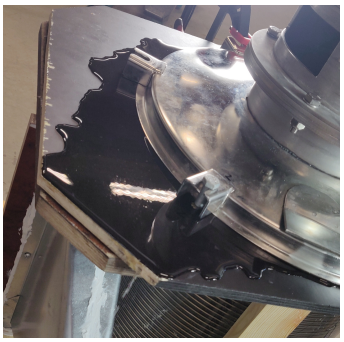
Figure 3.76: Water leaking out of the top lid cover at higher RPM.


Figure 3.77: The double gasket created to seal the top lid cover.

With the new double gasket seen in figure 3.77 installed, the testing resumed. Now, as the container no longer leaked, and it could handle high RPM up to around 300-325. At such high RPM, the mixer motor started to vibrate quite a lot, causing the entire container to move. Thankfully the entire container was bolted together with the mixer motor, so there was no danger of the impeller colliding with

the container walls. There was good flow through the pipes, but as expected, the bottleneck at the outlet caused the water flow to be bounced back and cause a vortex in the outlet nozzle. The cause for this is most likely because of the narrowness of the 2" outlet. The fact that the water bounces back here is a sign that the outlet cannot handle the output from the impeller, which means that with a wider outlet, one can expect a higher outflow. An ideal scenario would be to gradually increase the width of the outlet nozzle and observe where the flow no longer bounces back. At this point, the flow ought to be as laminar as possible inside the container.

Another thing observed during this test was that at high RPM, the water hit the outlet frame straight on and bounced back.

The issue with the wall in figure 3.78 could be easily remedied by creating a provisional cutwater. A cutwater is often something one can find inside a centrifugal pump. As its name suggests, its purpose is to cut the water and help make the flow towards the outlet as smooth as possible.

Figure 3.78: The outlet frame wall which caused turbulence at higher RPM.

With the cutoff seen in figures 3.79 and 3.80 installed, the water now flowed more nicely into the outlet. All in all, four water flow tests were conducted, 2 of which tested flow at 300RPM and over. As was expected in the theory section, cavitation did occur at high RPM. This was seen as tiny bubbles being formed inside the container, making the water look murky. These bubbles did not cause any apparent damage during the tests, but one can imagine that many tests with high RPM will start to impair the container's structural integrity.

Figure 3.79: The carved cutwater.

Overall the testing went better than expected, the container was completely watertight at the end, and it withstood all the forces inside it nicely. The decision to have the mantle wall transparent really did pay off, as one could easily witness everything going on inside the container. One could, for instance, see the areas of high turbulence and how they affected the flow. This concludes the experimental testing section.

Figure 3.80: The carved cutwater inserted at the outlet frame.

# 4

# *Results*

This results section consists of two parts, the CFD results, and the live experiment results.

## *4.1 CFD results*

This section involves the results recorded from the CFD simulations. It comes in chronological order as the models were developed, starting simple and progressively getting more complex.

### *4.1.1 2D simulations*

Below are the fluid velocities plotted from the first fluid simulations using laminar flow at 120RPM.

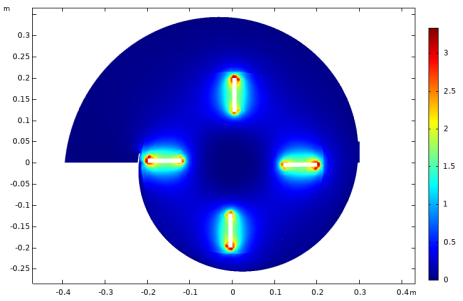

Figure 4.1: Fluid velocities at 0s.

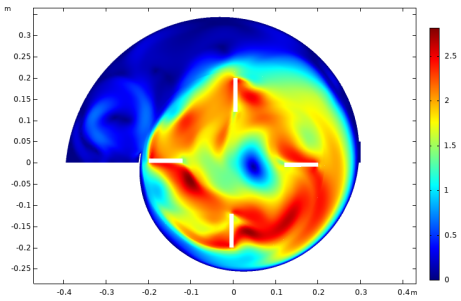

Figure 4.2: Fluid velocities at 2s.

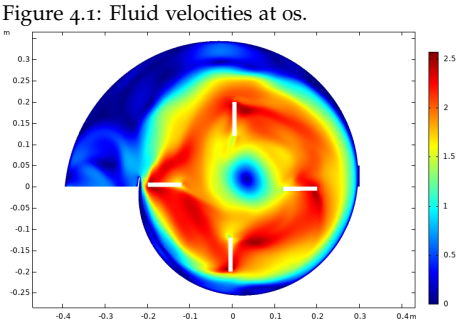

Figure 4.3: Fluid velocities at 6s.

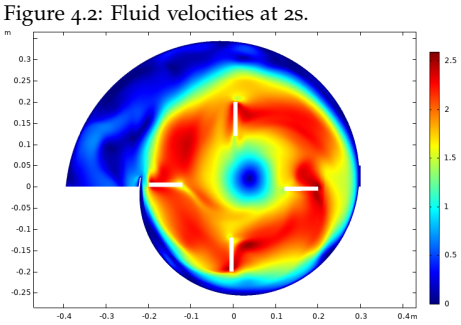

Figure 4.4: Fluid velocities at 8s.

Here in figure 4.1-4.4 one can get a quick glimpse of the behaviour of the fluid velocities inside the container. As can be seen, the velocities are quite tied to the inner domain of the impeller. At two seconds into the simulation in figure 4.2, one can see the velocities exhibit quite a chaotic behaviour, as to be expected when the fluid started stationary. As the simulation continues, one can notice in figures 4.3 and 4.4 that the fluid velocities become more balanced and rotate counter-clockwise nicely together with the four impeller wings, which is not what was expected. This is most indubitably a consequence of using the laminar flow physics model. This model works fine in simple cases such as water flowing through pipes, but in our case, where the fluid flow is expected to be more turbulent, something more robust is needed. Another consequence of using the laminar flow model is that it cannot handle fluid interactions near walls. This can be seen in, for instance, in figure 4.2, where the velocities never reach the edges of the walls, as if there was some invisible barrier there.

The same test with similar parameters was conducted using the Turbulent flow $k-\omega$ model, which gave the following results.

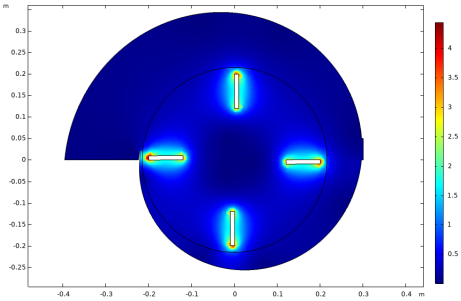

Figure 4.5: Fluid velocities at 0s.

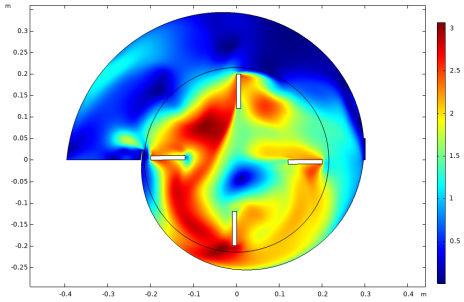

Figure 4.6: Fluid velocities at 2s.

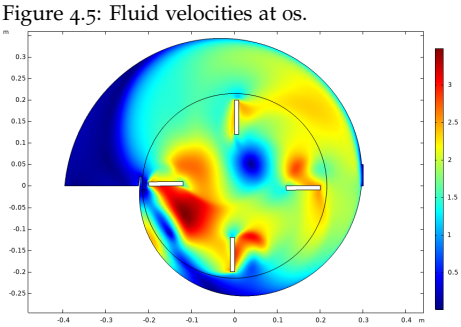

Figure 4.7: Fluid velocities at 6s.

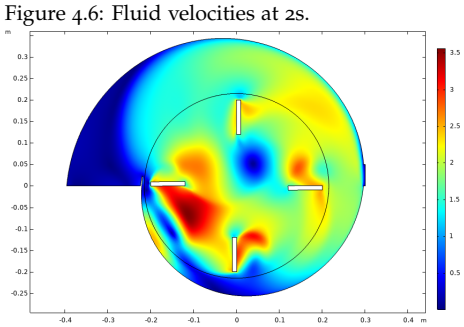

Figure 4.8: Fluid velocities at 8s.

In figures 4.5-4.8 one can instantly see that the model is much better at depicting the turbulent flow caused by the rotating impeller. However, it does look a bit more chaotic than expected. The flow exhibits a much more turbulent nature than the laminar flow test, which was good. The primary source of problems with both of these 2D simulations in hindsight is that the inlet is in a rather lousy location. Preferably it should be located at the center of the impeller.

### 4.1.2 3D Simulations: Container only.

Here are the results of the 3D CFD simulations. Starting with the first simple model, using the unoptimized spiral running at 60RPM.

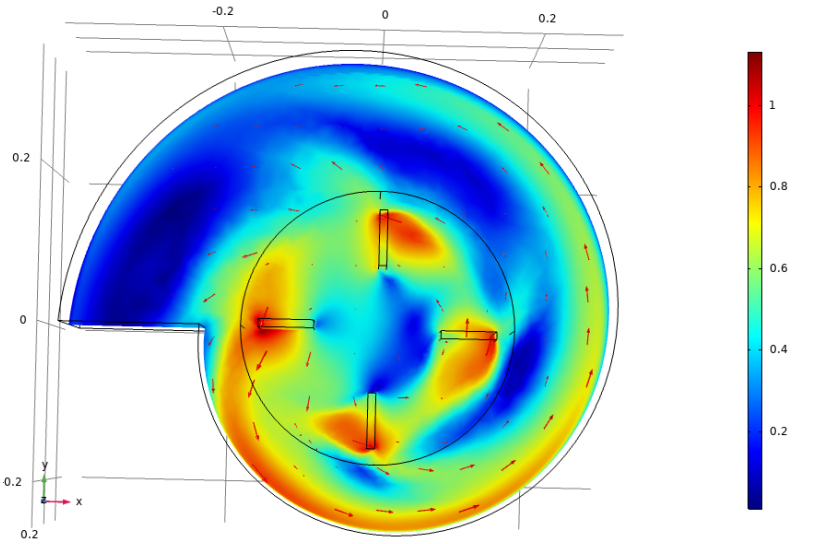


Figure 4.9: Fluid velocity of the simulation with rotational speed of 60RPM.

Here in figure 4.9 one can easily visualize the fluid velocity through a cross-sectional plane in the middle of the container. Unlike in the laminar flow case, the flow is now going in the right direction and traveling along the mantle wall of the spiral. It also becomes easy to see the effect of Bernoulli's Principle here. As the fluid goes from a tight area to a larger area, it will convert kinetic energy into pressure energy, which is visualized as the fluid losing velocity as it reached the outlet. This effect can be further seen in the pressure plot below.

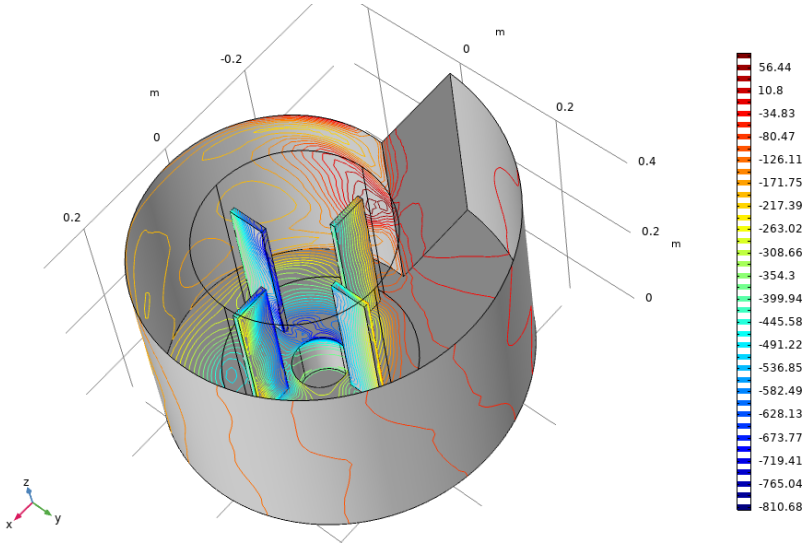


Figure 4.10: Fluid pressure at the walls.

As was expected, in figure 4.10 one can see that the pressure at the inlet is significantly lower than at the outlet. These simulations provide evidence that the spiral shape indeed seems to work as intended,

causing a pumping effect between the inlet and outlet of the container.

The velocities of 3D simulation using the optimized spiral are seen as follows, also running at 60RPM.

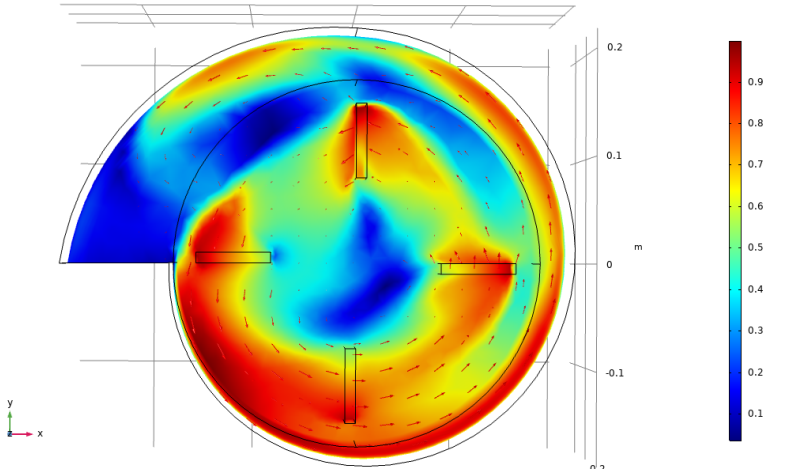


Figure 4.11: Fluid velocity of the container using the optimized spiral.

In figure 4.11 one can see the fluid velocities of the optimized spiral. Here it becomes more noticeable that the kinetic energy of the fluid is retained for a longer time compared to the design in 4.9. This was ideal as one must remember that the nozzle will still be added, causing an even more significant dip in kinetic energy. With this design, the velocity of the fluid should still be pretty high as it reaches the outlet.

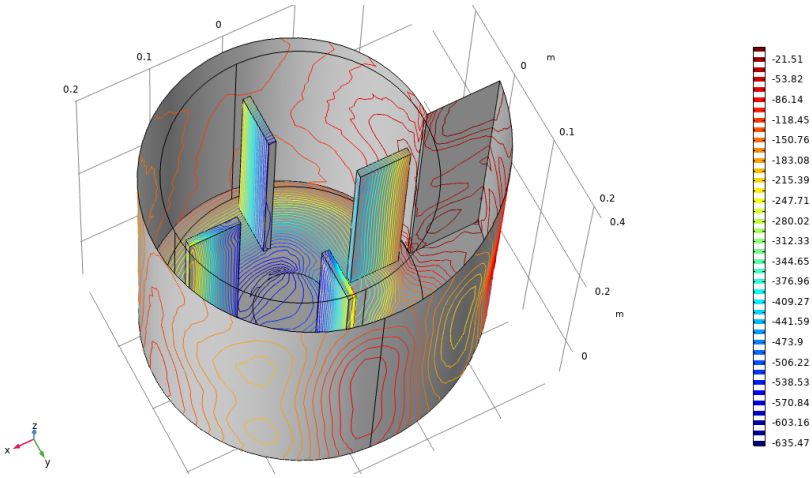


Figure 4.12: Fluid pressure at the edges of the container using the optimized spiral.

As expected, in figure 4.12 one can see that the pressure difference is lower than it is in figure 4.10. Thus meaning that the simulation has properly been able to depict the effects of Bernoulli's Principle.

## 4.2 3D Simulations: Container with hose

Here are the results from the tests where the container is connected to itself with a hose in a closed loop. These simulations are run on the model seen in figure 3.61.

### 4.2.1 240RPM

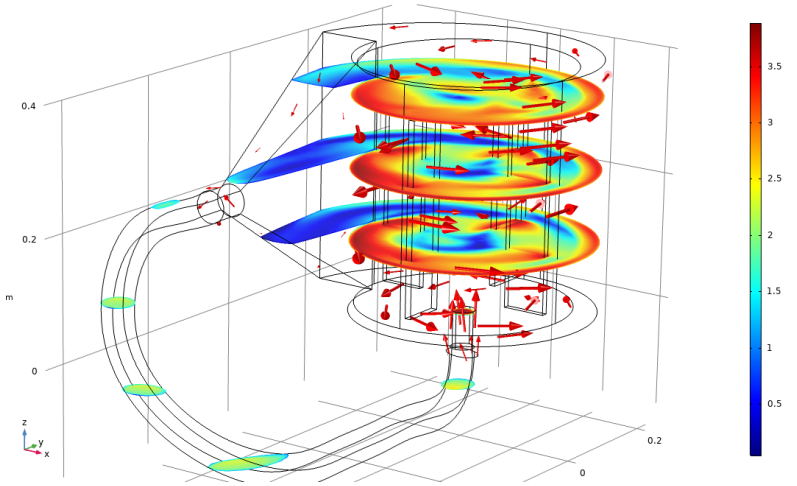


Figure 4.13: Fluid velocity plotted with surface arrows and 5 cut planes at 240RPM.

In figure 4.13 one can see the overall fluid velocities inside the container at 240RPM. From this, one can see that the fluid travels nicely from the inlet to the edge of the mantle and towards the outlet nozzle. It also becomes apparent that the outlet areal increase causes a high conversion from fluid kinetic energy to fluid pressure energy. To get a closer look at this, a cross-sectional cut plane at the middle of the container was analyzed.

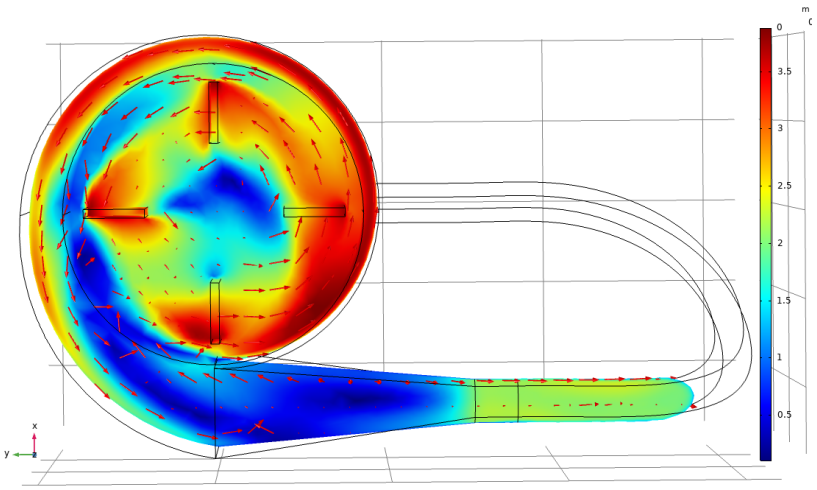


Figure 4.14: Fluid velocity plotted at a cut plane through the middle of the container. Surface arrows are normalized.

Figure 4.14 gives a much clearer picture of what is happening inside.

Do note that the surface arrows are normalized to give a clear picture of the flow direction inside the container. An interesting to note here is what is happening inside the outlet nozzle. As was expected, when the water reaches the outlet nozzle, it hits a bottleneck which causes the flow to become rather turbulent. One can, for instance, see that the flow is actually going back towards the container at one point, which is most likely the effect of a vortex forming at the outlet. One can also see that the fluid velocity gets faster at the hose, which is due to the fluid being constricted to a tighter space, converting pressure energy to kinetic energy. Going back to figure 4.13, one can see something interesting going on with the arrows at the outlet nozzle. A zoomed-in plot of the cut plane at this area was made.

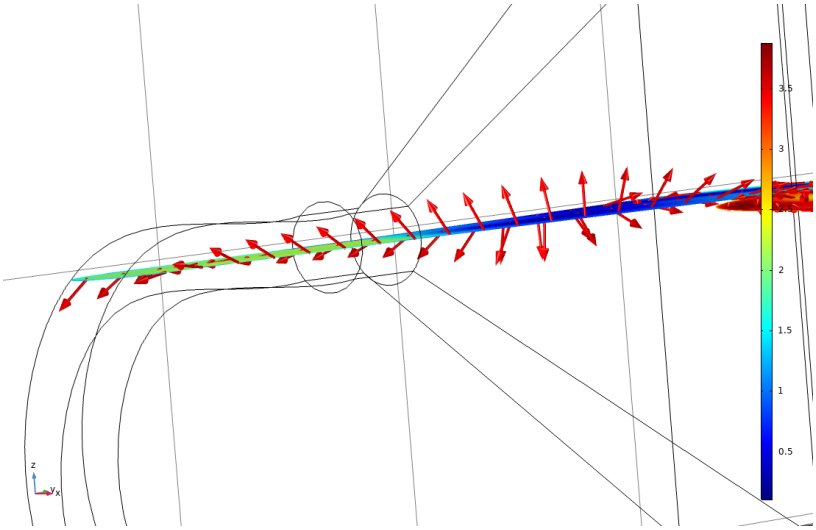

Figure 4.15: Fluid velocity and direction at the nozzle and hose.

In figure 4.15 one can see a zoomed-in view of the fluid velocity at the outlet nozzle and hose. Here one can see that the flow exhibits a rotational quality as it reaches the outlet nozzle. This is to be expected as it is an aftereffect of the water being set into rotation by the impeller.

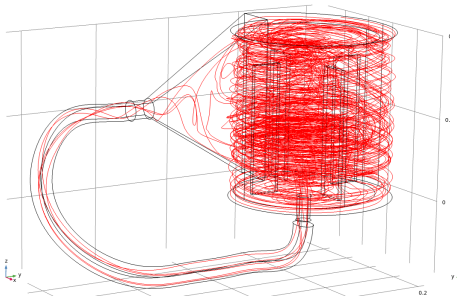
Figure 4.16: Streamline side view.

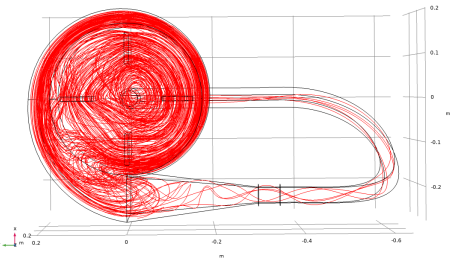
Figure 4.17: Streamline top view.

In figures 4.16 and 4.17, fluid velocity streamlines are plotted out to get a better idea of how the flow behaves inside the container. Here one can more easily visualize the vortex occurring at the center of the impeller and the rotational behaviour happening at the outlet nozzle.

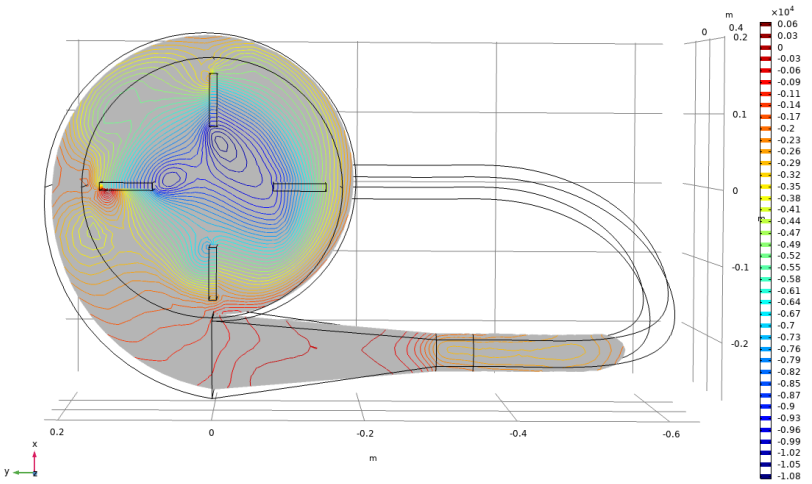


Figure 4.18: Fluid pressure plotted at a cut plane through the middle of the container.

Figure 4.18 shows the pressure gradient at the cut plane going through the middle of the container. As was expected, there exists a pressure difference between the center of the impeller and the outlet. This figure, together with figure 4.14 helps visualize the energy conversion within the fluid.

In these simulations, the flow rate was calculated by doing a surface integration of the velocity magnitude through a cut plane of the hose. This cut plane can be seen at figure 4.19. Flow rates were calculated at three different RPMs with this model.

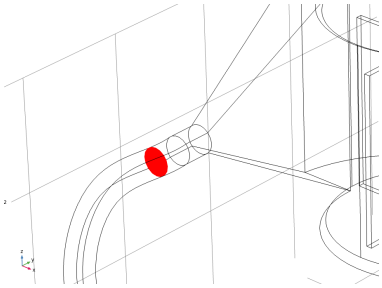

Figure 4.19: Cut plane where the flow rate was calculated.

Table 4.1: Flow rate in liters per second on the simplified 3D model with hose at three different RPM.

| RPM: | 120 | 180 | 240 |
|---|---|---|---|
| Flow rate: [l/s] | 2.02 | 2.99 | 4.14 |

Table 4.1 shows that this simplified model gives a reasonable flow rate of over 4 liters per second at 240RPM. As this seemed to be quite a high flow, it was determined that the complexity had to be increased in this model's geometry to depict the real-life scenario more appropriately.

### 4.2.2 *3D simulation: Final model*

These results are of the simulation using the model in figure 3.68. For brevity, the results plotted here are also of a simulation running at 240RPM.

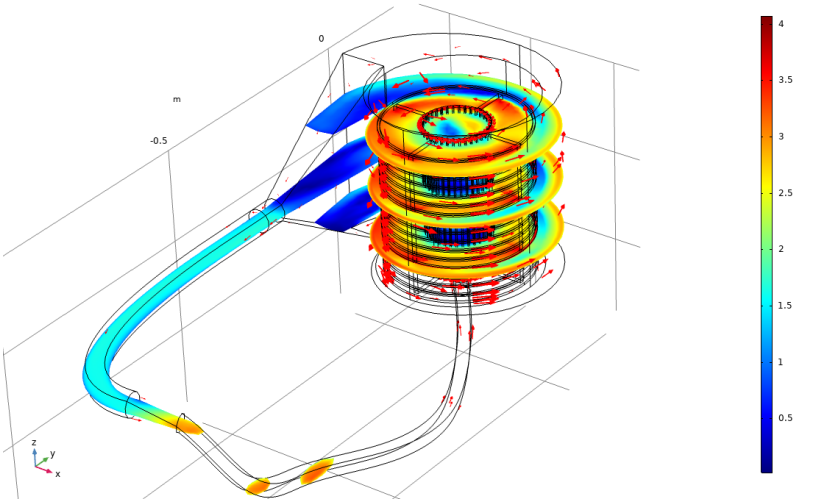


Figure 4.20: Fluid velocity plotted on the final model with surface arrows and 5 cut planes at 240RPM.

With the new impeller, one can see in figure 4.20 that the fluid velocity becomes more evenly distributed around surrounding the impeller compared to figure 4.13. This is indubitably due to the added geometries, which will cause more resistance in the fluid.

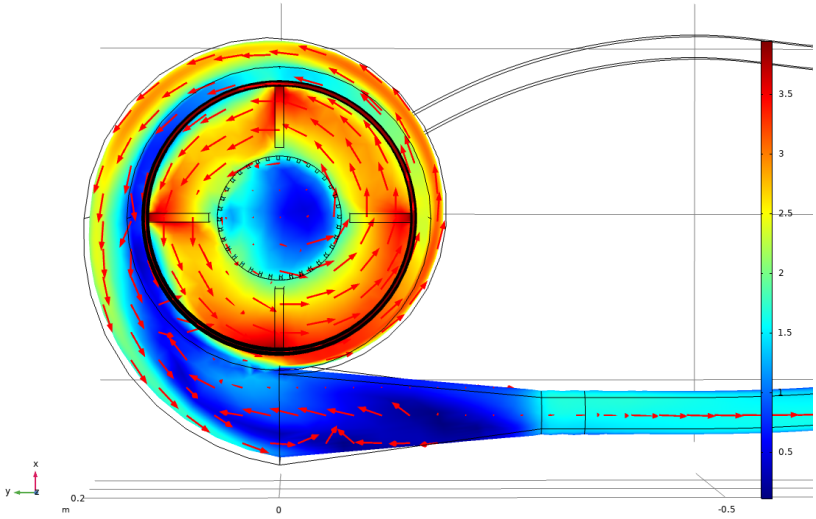


Figure 4.21: Cross section at the middle of the container, surface arrows are normalized.

In figure 4.21 it becomes apparent how the new impeller affects the fluid velocity. In figure 4.14 the flow was rather violent around the impeller, especially near the closest wall. However, now with the added cages, the flow becomes much more even inside the impeller, and it has a bit more issue in pushing out the fluid towards the mantle wall of the container. Here again, one can see the turbulent behaviour occurring inside the nozzle. To get a better view of this, a zoomed-in cross-section at the middle of the nozzle was made.

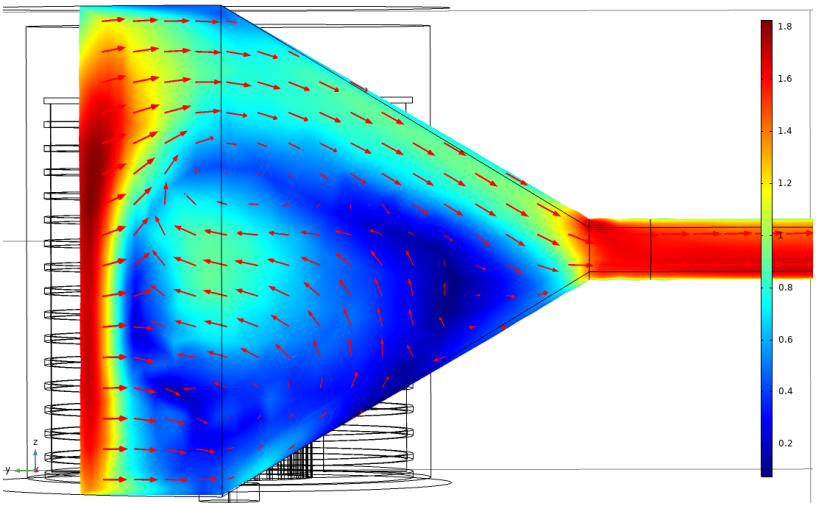


Figure 4.22: Cross section of the fluid velocity at the middle of the outlet nozzle, surface arrows are normalized.

Figure 4.22 gives a clear view of the turbulence formed inside the outlet nozzle. The water hits the bottom of the container, gets bounced back, and starts moving back towards the container. Another interesting detail is the flow at the top of the outlet. It seems very laminar and moves directly towards the hose.

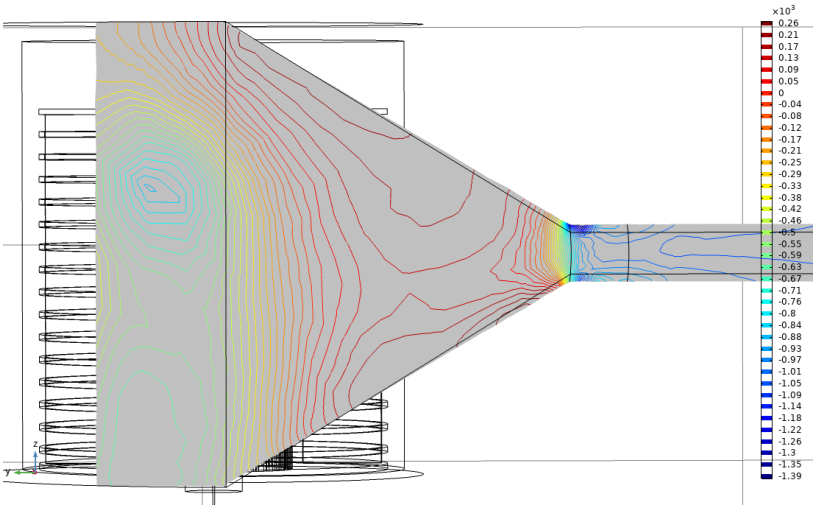


Figure 4.23: Cross section of the fluid pressure at the middle of the outlet nozzle.

The pressure at the nozzle in figure 4.23 paints a similar picture. The vortex caused by the turbulence creates an area of lower pressure at the entrance of the nozzle. Nevertheless, the pressure seems to continue to increase towards the end of the nozzle.

Values for the flow rate were calculated in a similar fashion as in the earlier simulations. The cut plane used for the calculations was at the same position where the flow sensor is in the real experiment.

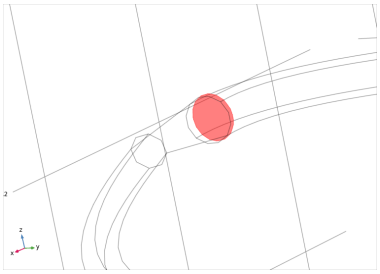

Figure 4.24: Position of the cut plane where the flow rate was calculated on the final model.

The flow rates calculated at the cut plane seen in figure 4.24 was calculated as follows.

Table 4.2: Flow rates for the final simulation model using the new impeller.

| RPM: | 118 | 188 | 245 |
|---|---|---|---|
| Flow rate: [l/s] | 1.38 | 2.21 | 2.9 |

Comparing the values in table 4.2 to those in table 4.1 one can see the effect the new impeller has on the flow rate of the container. With a drop in nearly 1 liter/second, it becomes apparent that the added complexity of the impeller caused a rather large change.

### 4.2.3 *Pressure development*

In order to further analyze how the pressure changes throughout the container, 18 3D cut points were plotted on the model. The points begin inside the hose, then to the inlet, through the impeller, and finally to the outlet.


Figure 4.25: Pressure changes as one goes from the hose (points 1-4) to the inlet(points 5-8), through the impeller (points 8-13) and towards the outlet (points 13-18).

Here in figure 4.25 one can see the successive pressure drops and gains that are similar to those seen in the theory of cavitation in figure 2.5. It displays that the flow pressure drops as it reaches the inlet and then increases towards the outlet. The pressures are negative since they are relative to the static pressure (1 atm).

## 4.3 *Testing results of the final design*

This section will cover the test results gathered from the real tests with the constructed container. All recorded values can be found in the appendix section.

### 4.3.1 *Test 1*

In the first test, the container started leaking from the top lid cover when reaching 160RPM, so the experiment was halted at that point. The recorded values and their averages can be seen at table 3 in the appendix.

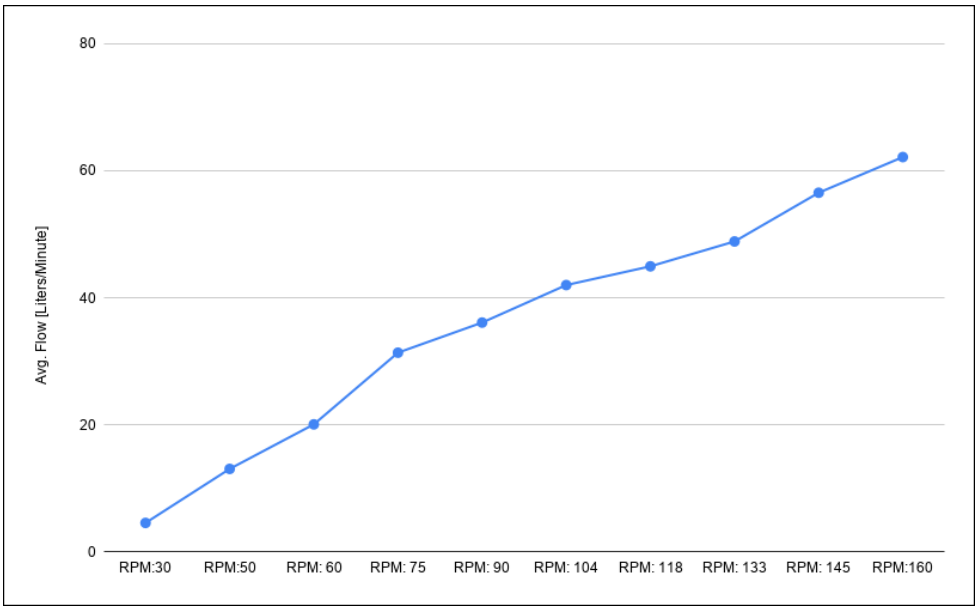


Figure 4.26: Average velocities as a function of RPM.

Figure 4.26 shows the development of the average flow as a function of the RPM. Already here, one can see that the flow behaves relatively linearly as one increases the RPM. At around 160RPM, the impeller was able to displace a little over 1 liter/second through the hose.

### 4.3.2 *Test 2*

At test 2, the top lid cover had been properly sealed and the carved cutoff installed. This experiment continued up until 260RPM, where the mixer motor started vibrating a bit too much, so the experiment was halted to inspect if any damages were caused to the container. The values can be seen at table 4 in the appendix. As earlier, this table also has the average flow through the sensor at each RPM level.

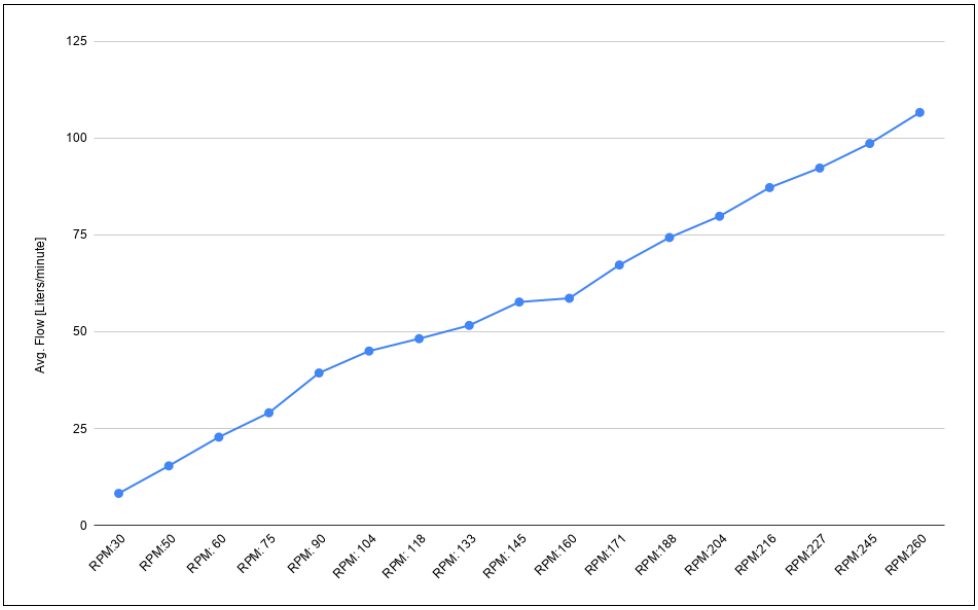


Figure 4.27: Average velocities as a function of RPM during the second test.

Figure 4.27 shows that the linear behaviour remains at higher RPM.

### 4.3.3 *Test 3*

With the structural integrity checked, the third test was done to push the RPM up to at least 300RPM. While there were heavy vibrations, the container handled them nicely. The results from this experiment can be seen in table 5. It is to be noted that cavitation bubbles were seen at around 270RPM. The average flow from this test was also calculated and can be found in the same table.

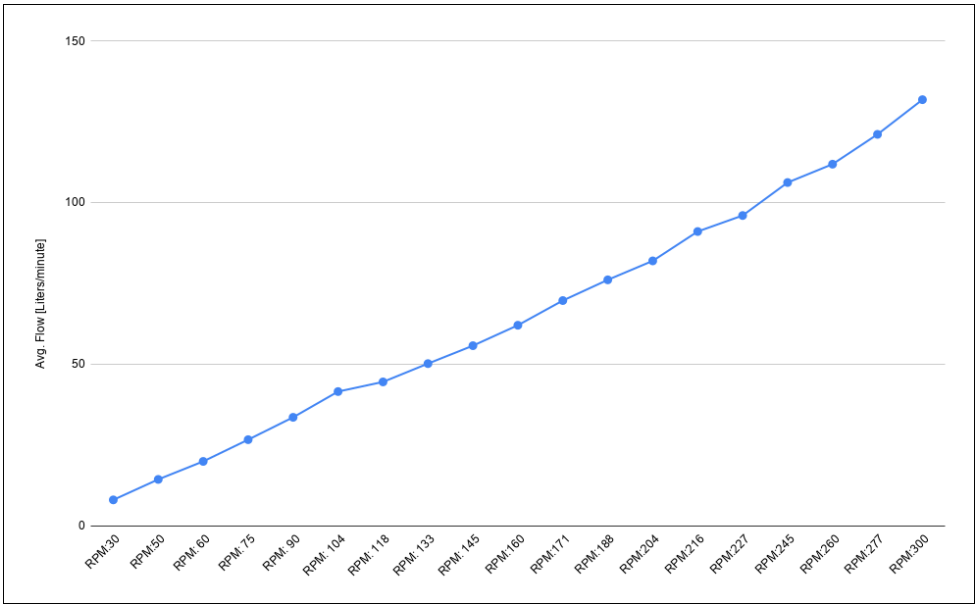


Figure 4.28: Average velocities as a function of RPM during the third test.

As expected, the linear behaviour continued. However, it was interesting to see that the formation of cavitation bubbles did not affect the flow rate as much as I had expected. Though prolonged testing at high RPM may result in damages to the impeller and container.

### 4.3.4 *Test 4*

During the last test, the mixer motor was pushed to its fastest setting, 325RPM. The results from the flow rate measurements and their averages can be seen found in table 6

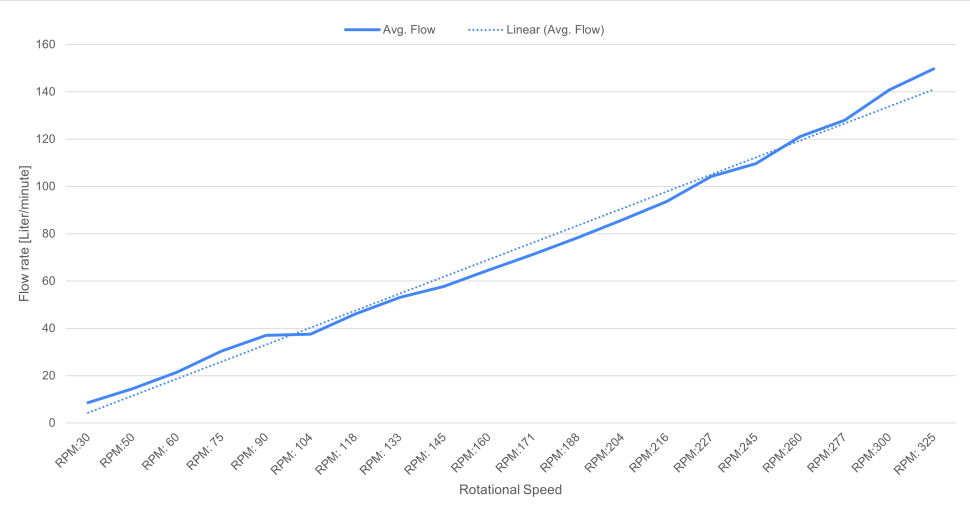


Figure 4.29: Average velocities as a function of RPM from the fourth test, together with a linear fit of the data.

In figure 4.29 one can see the averaged flow rate starting from the lowest possible setting to the highest on the mixer motor. As the results still show the linear behaviour, it was decided to conduct a linear fit on the data. The equation for the plotted linear fit is as follows

$$\text{Flow Rate [Liters/minute]} = 7.1953*\text{Rotational Speed [RPM]} - 2.8486\ . \tag{4.1}$$

The equation for the linear fit in equation 4.1 shows a linear approximation of how the flow rate changes as a function of the rotational speed. Comparing the results from the real-life test to the results of the final CFD simulations, one can see that they have quite a large difference. For instance, the flow rate at 245RPM in the simulation was 2.9 liters per second, whereas the flow in the real test with the same RPM was at an average of 1.76 liters per second.

In order to get a more detailed comparison between the CFD and the real-life results, several simulations were conducted using the same rotational velocities as in test 4. This comparison was made from 60 RPM to 300 RPM. This can be visualized in the following plot

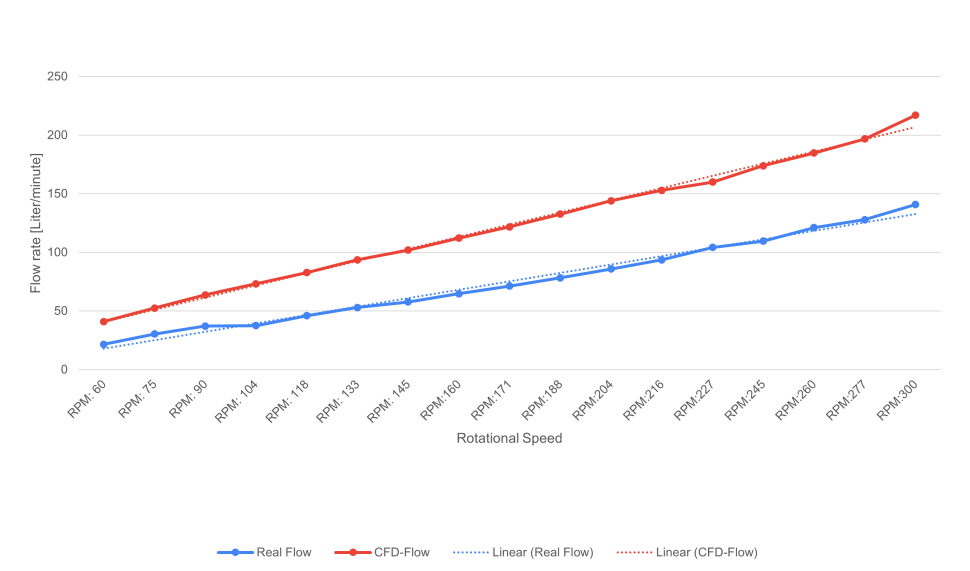


Figure 4.30: Comparison between the CFD flow rate (red) and real life flow rate (blue).

Figure 4.30 shows that while there exists a difference between the flow rates between the CFD simulations and the real test, the linear trend persists. This is a good indicator that the simulation does indeed mimic reality well. The differences in flow rate probably arise from factors such as the real-life impeller being more complex than the CFD impeller or the resistance caused by the propellers in the flow sensor. As these two comparisons used fewer data points, new linear fits were made on both. The following equations were developed from the respective linear fits.

$$\text{Flow Rate CFD [Liters/minute]} = 10.393*\text{Rotational Speed [RPM]} + 30.287 \quad (4.2)$$

$$\text{Flow Rate Real [Liters/minute]} = 7.174*\text{Rotational Speed [RPM]} + 10.788 \quad (4.3)$$

One can see that the difference in the slope from equation 4.2 and equation 4.3 is around 3,22. Thus, this indicates that the CFD simulations' slope is around 36% higher than in the real-life scenario.

## 4.4 Discussion

The progress throughout this project was fairly different from my initial expectations at the start. At the start of the project, I felt a bit like a fish out of water, as many tasks were outside my field of expertise. However, I tried not to let that fact discourage me and instead saw it as an opportunity to learn and acquire new skills. By utilizing all the skills I have gathered through my years as a student, especially the skill of adequately tackling problems and solving them efficiently, I organized my thoughts and tried to set my focus on solving one problem at a time. With a project like this, it can be easy to get overwhelmed with all of the tasks at hand. This case was particularly relevant at around the halfway point through the project when it was decided that I build the container myself. By keeping a calm mind and with the help from my supervisor, I got through this problem relatively smoothly. The construction phase initially intimidated me but turned out to be the part of the project where I had the most fun. It took about two months of work to fully build the container and set it up for testing, granted it was a bit longer than I had initially planned. One thing I definitely learned was that one should not put too much faith in initial estimations on projects like this, as sudden changes or setbacks can occur at any moment. For the CFD simulations, I also had a good time tackling the more physics-related problems of the project. While I still consider myself a novice in the field, I do feel like I learned a lot when it comes to fluid simulations. Many painstaking hours were spent trying to get a mesh to work or figuring out why a simulation never converged, each problem solved in due course.

When it comes to improvements in the design, I had a couple of ideas in mind. The outlet nozzle seemed to cause a lot of turbulence in the flow, which meant that instead of getting directed towards the end of the outlet, the flow instead started to go back into the container. In the best-case scenario, the flow would be perfectly laminar at the outlet and go smoothly into the connecting hose. An idea could be to install baffles along the outlet nozzle in order to reduce the turbulent behaviour of the flow. It would also be interesting to see how the flow rate would behave if a bigger hose was used. Another glaring problem with the design was the hole for the shaft in the top lid veneer sheet. At higher RPM, water started entering through this hole and into the space between the sheet and top lid cover. A fix for this could be done by designing a module that covered the shaft and then constructing it with the help of a 3D printer. This module would encompass the shaft and surround it with a fitting gasket so that no water would be able to get through. As the container was designed around the idea of a centrifugal pump but consequently designed to fit the impeller, it gave the container a more elongated structure. Actual centrifugal pumps are often relatively flat, with very little dead space between the impeller and container walls. Therefore as my de-

sign almost takes the shape of a tank, one can imagine that the flow may get a bit turbulent along the container walls. The simulations showed that the flow is fairly smooth, but I believe improvements could be made here. As with the case of the outlet nozzle, one could install horizontal baffles along the spiraling mantle wall to further guide the flow and reduce turbulence. Another interesting idea I thought of when analyzing classical centrifugal pumps was the addition of a diffuser. The diffusers are sometimes used in larger centrifugal pumps and are a set of stationary vanes that surround the impeller. These vanes help increase the overall pumping efficiency by reducing the flow velocity and, in consequence, increase the fluid pressure.

Naturally, in the CFD simulations, an obvious future development would be to include some porous material inside the impeller. This would simulate how the flow behaves during an actual purification, and one could get a better idea of how much it affects the flow rate. As seen in figure 4.22 the flow is focused at the top part of the outlet nozzle. A reason for this may be because of the position of the impeller on the z-axis inside the container. Further studies could then be conducted on seeing what kind of impact this parameter has on the flow pattern inside the outlet nozzle.

From the results gathered of the flow rates, both from the CFD simulations and the real-life testing, indicate that there does indeed exist potential for this container design. The centrifugal pump design acted as expected and correctly converted the kinetic fluid energy caused by the impeller to fluid pressure energy as it reached the outlet nozzle. However, there was quite a discrepancy between the simulated CFD flow rates and the flow rates acquired from the actual tests. I could think of a few factors that explained this difference. First and foremost, the complexity of the impeller. In the CFD simulations, computational power limitations resulted in me having to use a simplified model for the impeller. In reality, the impeller has quite a complex and detailed geometry which can be very difficult to simulate. A specific detail is the sift-type structure along the walls of the impeller, which keeps the ion-exchange resin inside the impeller. These sifts are very thin and closely packed. A potential solution for properly simulating this is by creating an area surrounding the impeller model that had some resistance to it that mimicked the resistance caused by the sift. I think that if this was done, the flow rate would get closer to reality. Another thing was the actual flow sensor inside the pipe, the fins measuring the flow would indubitably cause a resistance, consequently causing a lower flow rate. Again this could be implemented into the simulation by adding an equal flow resistance at the same area one has the cut plane for the flow rate calculations.

## 4.5 Conclusion

The main conclusion drawn from this project is that the spiral shape design of the container did indeed result in a pump effect between the outlet and inlet. With the elongated centrifugal pump design built around the specified impeller, one can achieve both a good outflow in the system and keep the container relatively compact easily transportable. It should be possible to connect this type of system to any type of tank and conduct remediation of contaminated fluids. The design can be built in steel with the blueprints but can also be built significantly cheaper using materials like wood and plastic. However, by choosing cheaper materials, the consequence is that it becomes bulkier to make up for its lack of structural integrity. This container allows the user to utilize the benefits of the rotating bed reactor without having to insert it directly into tanks filled with potentially hazardous liquids, significantly increasing ergonomics in work environments where it can be otherwise difficult to conduct a purification process. As discussed in the introduction of this project, the developed design could potentially be utilized in the purification of radioactive wastewater in nuclear power plants. Having a system that provides an easy and safe alternative to purify irradiated water could give further incentive for nations to invest in nuclear energy.

The results from the CFD simulations shone a light on the weaknesses of the final design and could be used as a starting point in further research. For instance, the flow and pressure occurring inside the outlet nozzle showed that one might want to find a way to optimize the flow in this area to prevent the high turbulent behaviour of the fluids. One could also get a good idea of the impact the geometry of the impeller had on the overall flow rate in the system. The more you cover up the four wings inside the impeller, the lower your flow rate will become. Overall the simulations gave extra proof that the conversion of kinetic energy to pressure energy in the tank worked as expected inside the container.

Overall the results from both the real-life testing and the CFD simulations show that the proposed design works as intended. As the design is not overly complex, it could quite easily be built in mass scale. The container with a mixer motor and the impeller could provide industries with a practical way of dealing with contaminated water, further driving humanity towards achieving a fully sustainable environment.

# .1 Appendix

Appendix for the project.

## .1.1 *Blueprints for the container components.*

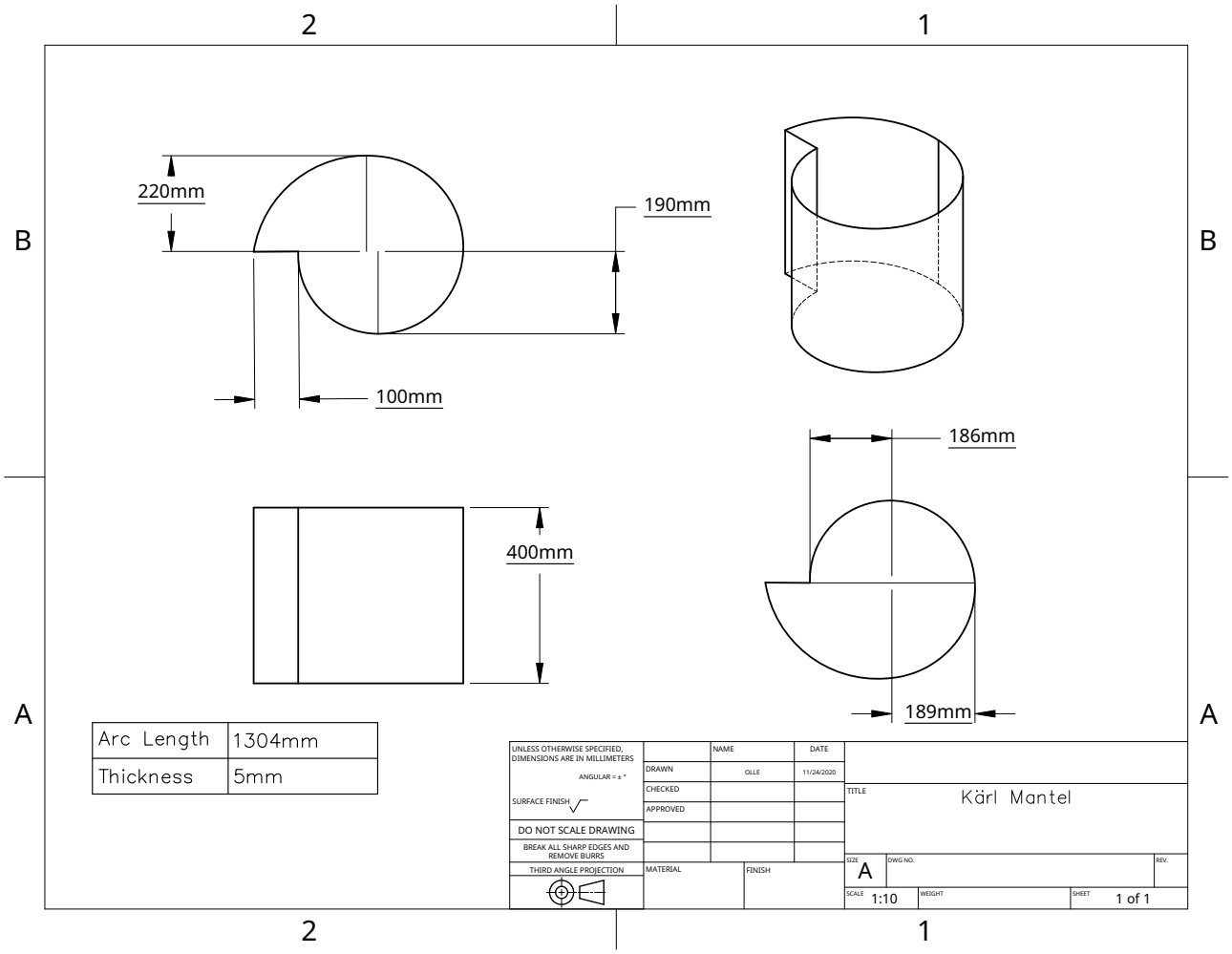


Figure 31: Blueprint for the mantle of the container.

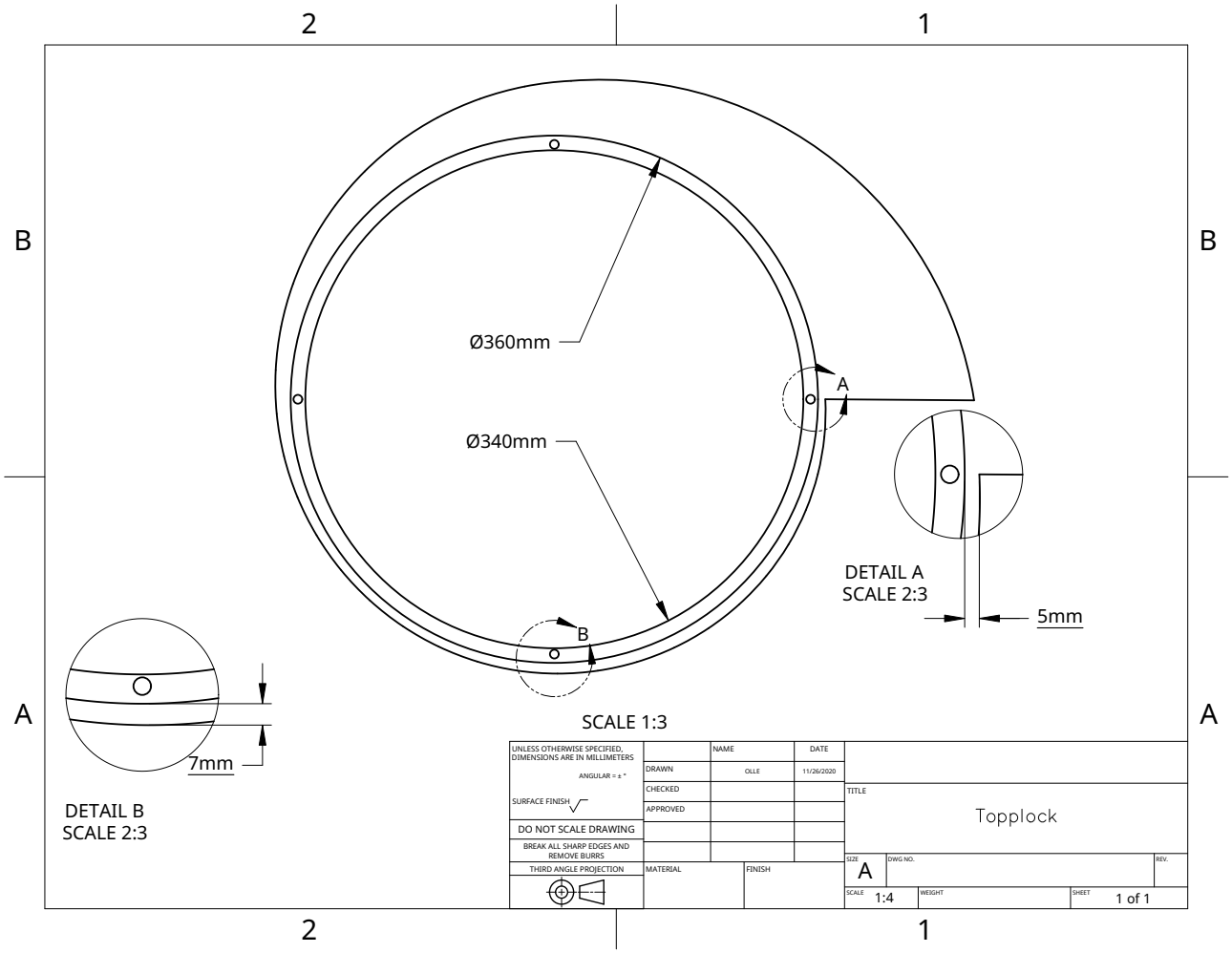


Figure 32: Blueprint 1 for the top lid of the container.

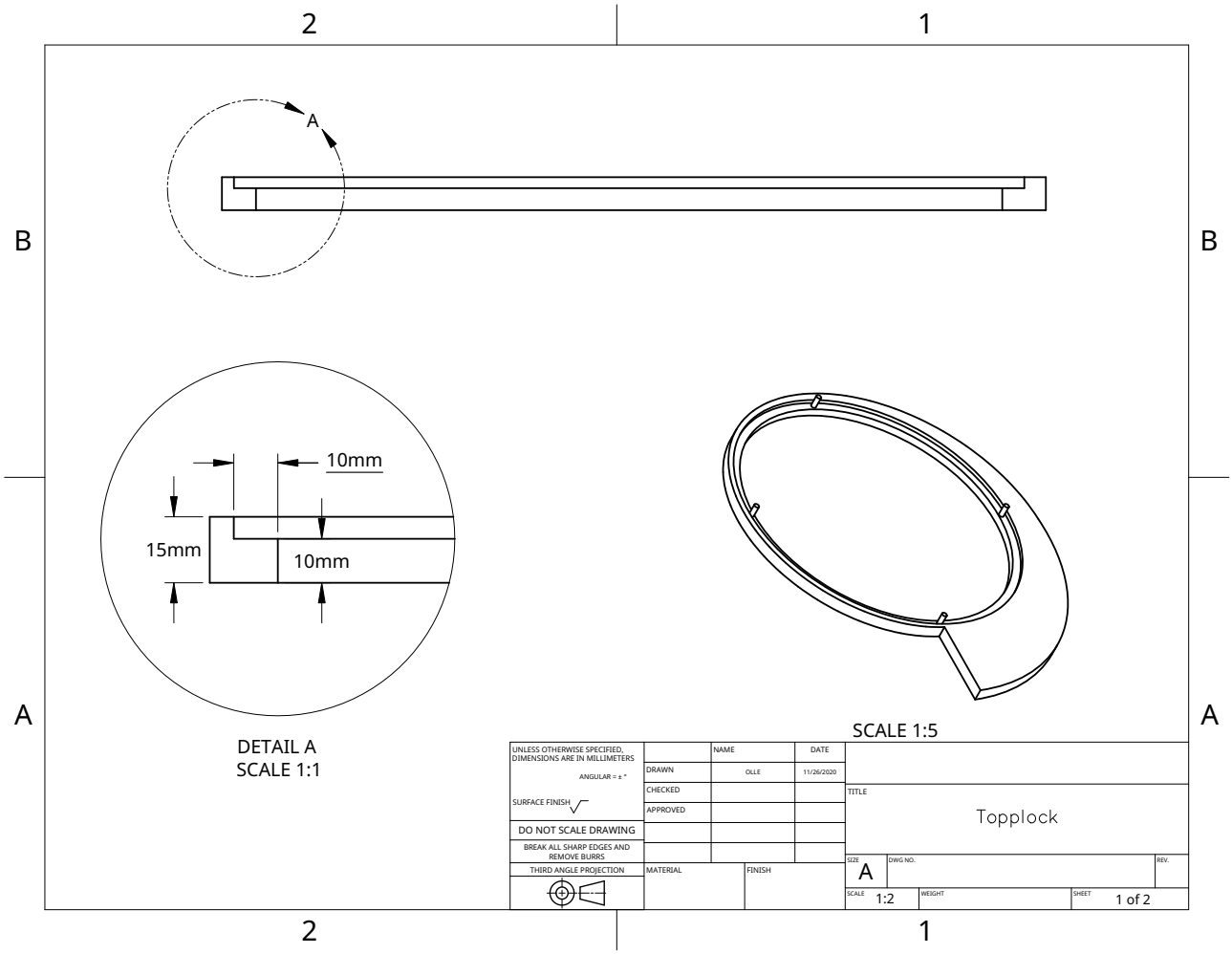


Figure 33: Blueprint 2 for the top lid of the container.

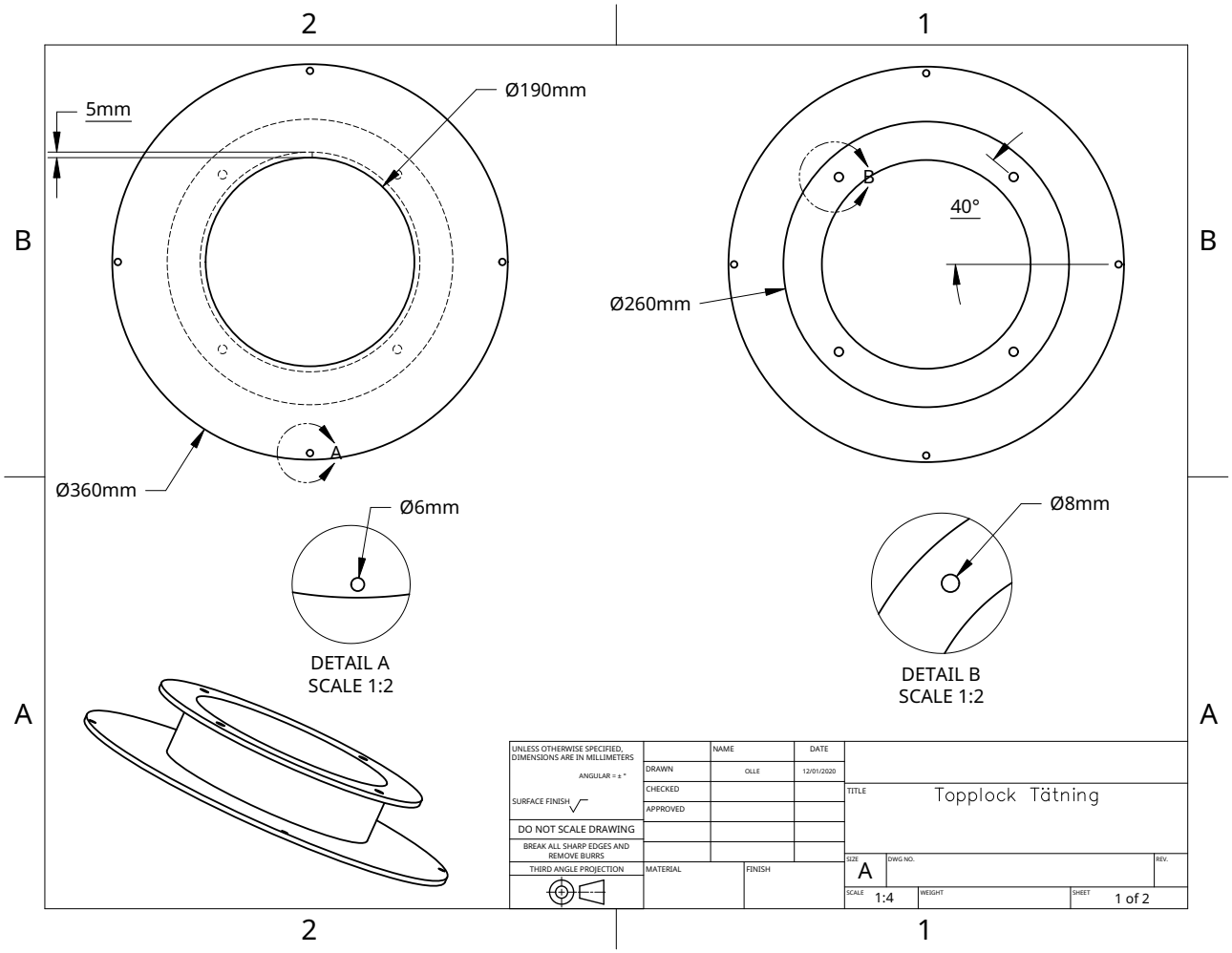


Figure 34: Blueprint 1 for the top lid cover of the container.

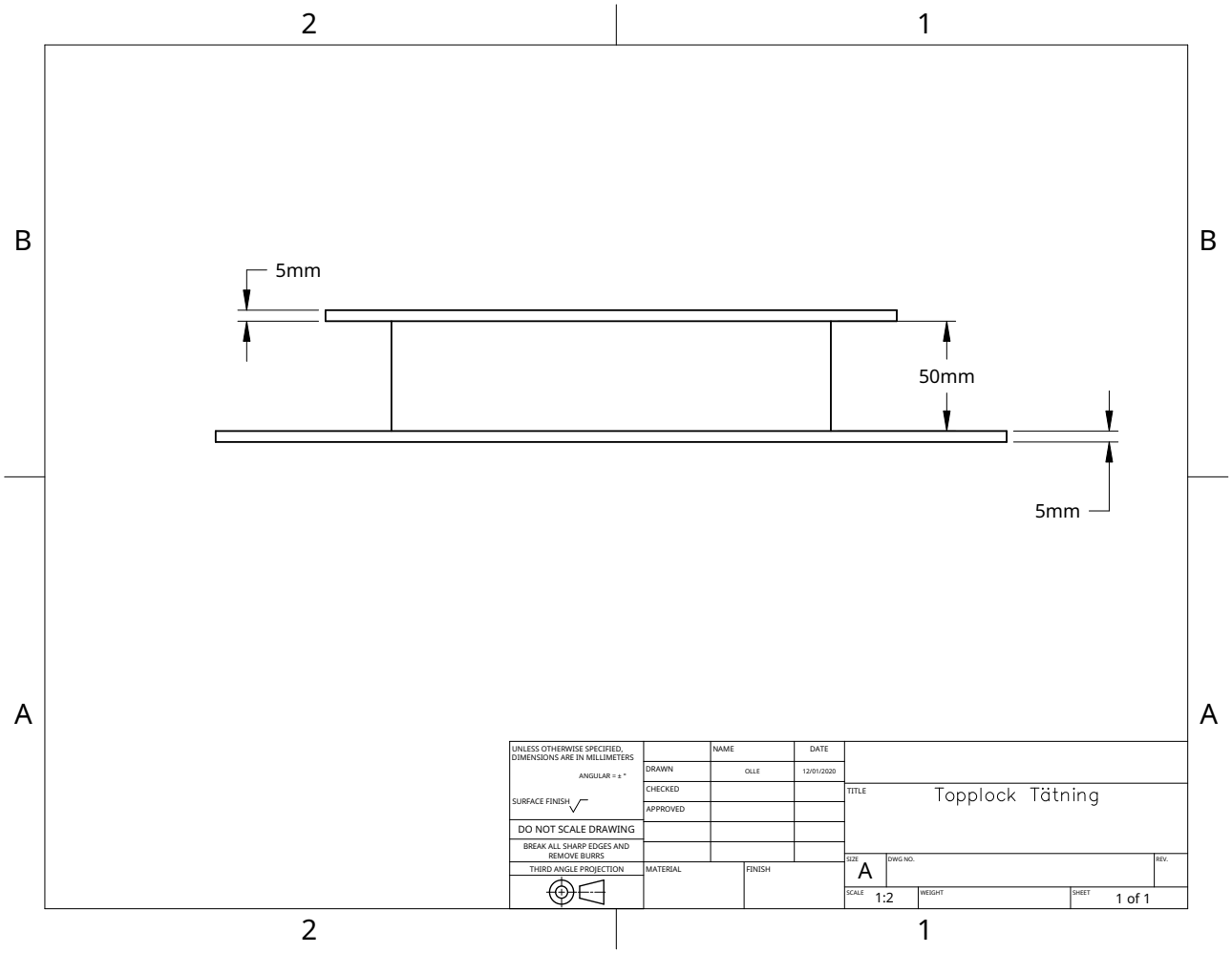


Figure 35: Blueprint 2 for the top lid cover of the container.

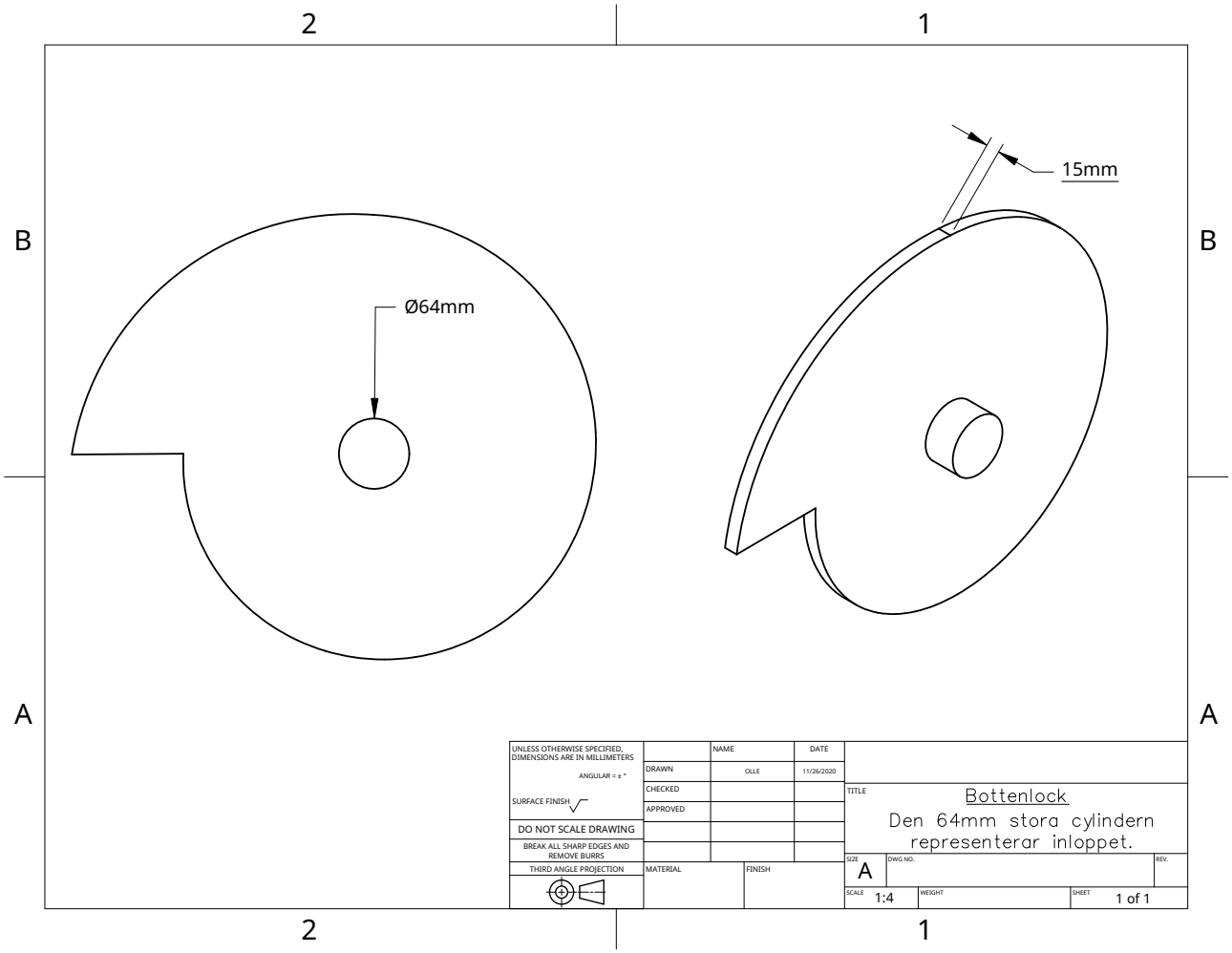


Figure 36: Blueprint for the bottom lid of the container.

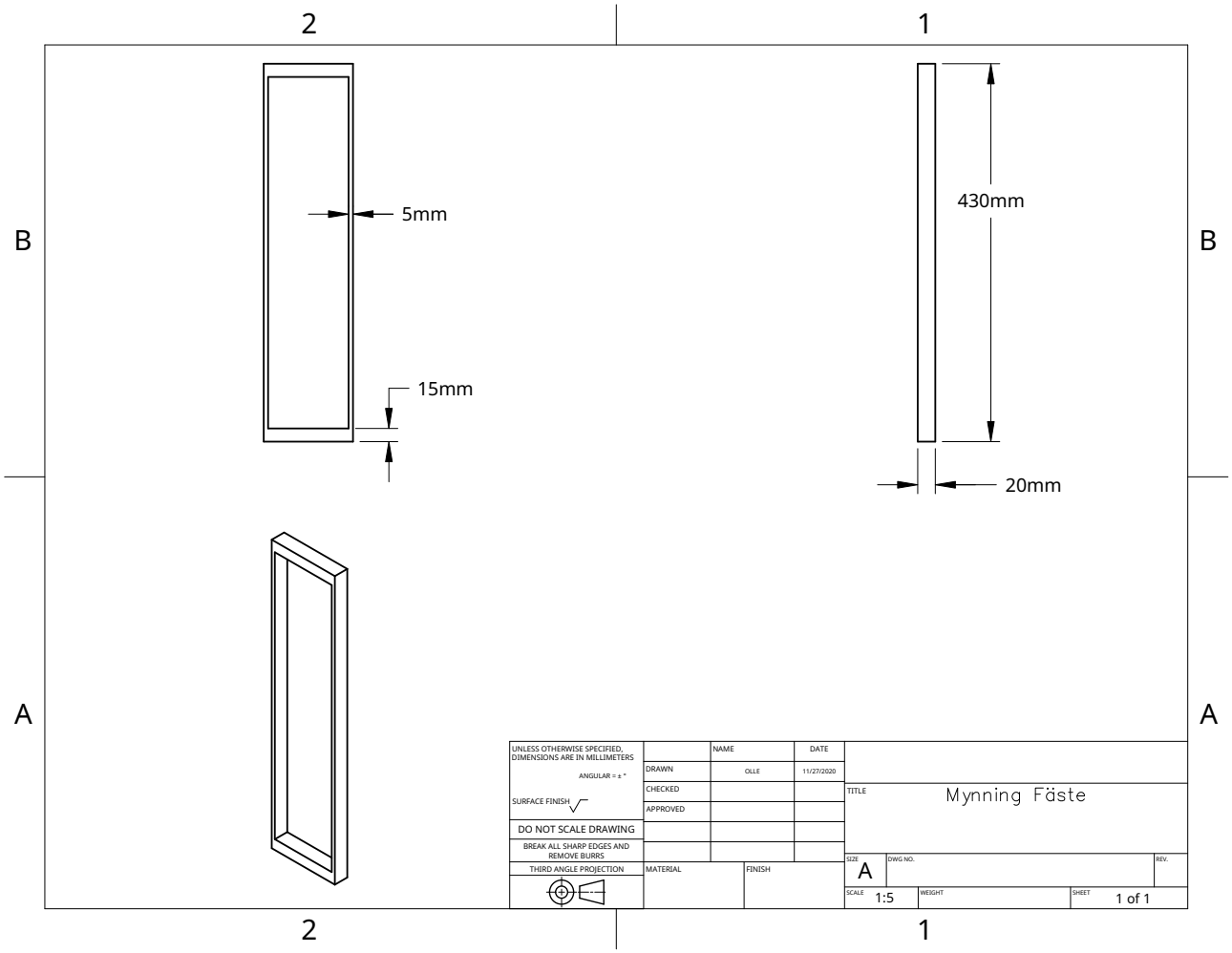


Figure 37: Blueprint for the outlet nozzle frame.

### .1.2 *Test Results*

## *Test 1*

Table 3: Flow rate results and averages from the first test, measured in liters per minute.

| | Flow [l/minute] | Flow [l/minute] | Flow [l/minute] | Avg. Flow |
|---|---|---|---|---|
| RPM:30 | 4,29 | 4,88 | 4,19 | 4,585 |
| RPM:50 | 12,51 | 13,66 | 12,85 | 13,085 |
| RPM: 60 | 20,26 | 19,92 | 19,75 | 20,09 |
| RPM: 77 | 25,8 | 36,93 | 25,88 | 31,365 |
| RPM: 90 | 35,88 | 36,32 | 35,95 | 36,1 |
| RPM: 104 | 41,78 | 42,22 | 40,58 | 42 |
| RPM: 118 | 45,12 | 44,78 | 44,3 | 44,95 |
| RPM: 133 | 48,61 | 49,11 | 48,92 | 48,86 |
| RPM: 145 | 54,85 | 58,2 | 56,3 | 56,525 |
| RPM:160 | 62,55 | 61,72 | 63,17 | 62,135 |

## *Test 2*

Table 4: Flow rate results and averages from the second test, measured in liters per minute.

| | Flow [l/minute] | Flow [l/minute] | Flow [l/minute] | Avg. Flow |
|---|---|---|---|---|
| RPM:30 | 8,53 | 8,01 | 8,69 | 8,27 |
| RPM:50 | 15,12 | 15,63 | 15,15 | 15,375 |
| RPM: 60 | 23,24 | 22,36 | 22,06 | 22,8 |
| RPM: 75 | 29,05 | 29,11 | 30,21 | 29,08 |
| RPM: 90 | 39,18 | 39,55 | 38,19 | 39,365 |
| RPM: 104 | 45,87 | 44,18 | 45,66 | 45,025 |
| RPM: 118 | 47,12 | 49,32 | 47,37 | 48,22 |
| RPM: 133 | 51,08 | 52,21 | 53,07 | 51,645 |
| RPM: 145 | 57,17 | 58,2 | 56,72 | 57,685 |
| RPM:160 | 59,98 | 57,33 | 59,45 | 58,655 |
| RPM:171 | 66,34 | 68,16 | 69,06 | 67,25 |
| RPM:188 | 74,18 | 74,51 | 72,3 | 74,345 |
| RPM:204 | 79,55 | 80,12 | 79,74 | 79,835 |
| RPM:216 | 85,91 | 88,57 | 85,98 | 87,24 |
| RPM:227 | 91,9 | 92,67 | 94,07 | 92,285 |
| RPM:245 | 99,5 | 97,75 | 101,11 | 98,625 |
| RPM:260 | 105,9 | 107,38 | 110,61 | 106,64 |

## *Test 3*

Table 5: Flow rate results and their averages from the third test, measured in liters per minute.

| | Flow [l/minute] | Flow [l/minute] | Flow [l/minute] | Avg. Flow |
|---|---|---|---|---|
| RPM:30 | 8,19 | 7,96 | 7,99 | 8,046666667 |
| RPM:50 | 14,16 | 14,46 | 14,51 | 14,37666667 |
| RPM: 60 | 20,38 | 19,45 | 20 | 19,94333333 |
| RPM: 75 | 26,43 | 26,69 | 26,88 | 26,66666667 |
| RPM: 90 | 33,26 | 33,2 | 34,28 | 33,58 |
| RPM: 104 | 41,15 | 41,28 | 42,21 | 41,54666667 |
| RPM: 118 | 43,08 | 44,92 | 45,59 | 44,53 |
| RPM: 133 | 51,2 | 50,05 | 49,33 | 50,19333333 |
| RPM: 145 | 56,17 | 55,92 | 55,12 | 55,73666667 |
| RPM:160 | 62,61 | 61,5 | 62,07 | 62,06 |
| RPM:171 | 68,91 | 69,06 | 71,12 | 69,69666667 |
| RPM:188 | 75,35 | 76,68 | 76,27 | 76,1 |
| RPM:204 | 82,16 | 81,3 | 82,44 | 81,96666667 |
| RPM:216 | 89,28 | 93,2 | 90,66 | 91,04666667 |
| RPM:227 | 95,32 | 96,15 | 96,52 | 95,99666667 |
| RPM:245 | 104,15 | 105,05 | 109,4 | 106,2 |
| RPM:260 | 110,37 | 112,13 | 113,12 | 111,8733333 |
| RPM:277 | 122,33 | 119,47 | 121,5 | 121,1 |
| RPM:300 | 132,37 | 130,22 | 132,89 | 131,8266667 |

## *Test 4*

Table 6: Flow rate and average flow results from the fourth test, measured in liters per minute.

| | Flow [l/minute] | Flow [l/minute] | Flow [l/minute] | Avg. Flow |
|---|---|---|---|---|
| RPM:30 | 8,75 | 8,59 | 8,56 | 8,633333333 |
| RPM:50 | 14,56 | 14,49 | 14,59 | 14,54666667 |
| RPM: 60 | 21,35 | 21,51 | 21,72 | 21,52666667 |
| RPM: 75 | 30,2 | 30,41 | 30,46 | 30,35666667 |
| RPM: 90 | 37 | 37,27 | 37,07 | 37,11333333 |
| RPM: 104 | 37,93 | 36,88 | 37,83 | 37,54666667 |
| RPM: 118 | 45,33 | 46,62 | 46,1 | 46,01666667 |
| RPM: 133 | 53 | 52,16 | 54,04 | 53,06666667 |
| RPM: 145 | 56,27 | 58,13 | 58,84 | 57,74666667 |
| RPM:160 | 65,1 | 64,22 | 64,85 | 64,72333333 |
| RPM:171 | 71,62 | 71,12 | 71,17 | 71,30333333 |
| RPM:188 | 77,02 | 78,61 | 79,3 | 78,31 |
| RPM:204 | 86,28 | 85,25 | 86,02 | 85,85 |
| RPM:216 | 95,6 | 92,08 | 93,37 | 93,68333333 |
| RPM:227 | 104,52 | 102,45 | 105,82 | 104,2633333 |
| RPM:245 | 109,17 | 111,23 | 108,45 | 109,6166667 |
| RPM:260 | 119,47 | 123,19 | 120,62 | 121,0933333 |
| RPM:277 | 127,76 | 127,75 | 128,4 | 127,97 |
| RPM:300 | 144,14 | 140,05 | 138,5 | 140,8966667 |
| RPM:325 | 149,42 | 151,28 | 148,63 | 149,7766667 |

# *Bibliography*


[1] World Population Growth, Hannah Ritchie, Max Roser and Esteban Ortiz-Ospina, 2013. Available at: https://ourworldindata.org/world-population-growth

[2] Water Use and Stress, with data from the Global International Geosphere-Biosphere Programme (IGB), Hannah Ritchie, 2017. Available at: https://ourworldindata.org/water-use-stress

[3] World Population Growth, with data from the United Nations Populations Division, Max Roser, Hannah Ritchie and Esteban Ortiz-Ospin, 2013 Available at: https://ourworldindata.org/world-population-growth

[4] United Nations Environment Programme. Vital Water Graphics—An Overview of the State of the World's Fresh and Marine Waters, 2nd ed.; UNEP: Nairobi, Kenya, 2008.

[5] Cooling for electricity production dominates water use in industry, Jürgen Förster, 2014.
Available at: https://op.europa.eu/en/publication-detail/-/publication/ac2b6f1d-9270-4010-bbaf-3834ac2d6ee2

[6] A global, spatially-explicit assessment of irrigated croplands influenced by urban wastewater flows, A L Thebo, P Dreschel, E F Lambin and K L Nelson, 2017.
Available at: https://iopscience.iop.org/article/10.1088/1748-9326/aa75d1/pdf

[7] Nonfossil sources accounted for 20% of U.S. energy consumption in 2019, U.S. Energy Information Administration, 2019. Available at: https://www.eia.gov/todayinenergy/detail.php?id=44277

[8] Annual Energy Outlook 2020, U.S. Energy Information Administration, 2020. Available at: https://www.eia.gov/outlooks/aeo/pdf/AEO2020%20Full%20Report.pdf

[9] World Nuclear Performance Report 2020, World Nuclear Association, 2020. Available at: https://www.world-nuclear.org/getmedia/3418bf4a-5891-4ba1-b6c2-d83d8907264d/performance-report-2020-v1.pdf.aspx

[10] Energy Issues in Sustainable Urban Wastewater Management: Use, Demand Reduction and Recovery in the Urban Water Cycle, Andrea G. Capodaglio and Gustaf Olsson, 2016. Available at: http://www.jwsponline.org/uploadpic/Magazine/Volume%206%20Issue%202%20%20%20pp63-76.pdf

[11] Agitator Introduction, CEM(Changzhou) Special Equipment CO., Ltd. 2012 Available at: http://www.cemspe.com/english/products.asp-action=Detail&id=288.htm

[12] Which Impeller Is Right for Your Cell Line?, Rich Mirro and Kevin Voll, 2009. Available at: https://bioprocessintl.com/analytical/cell-line-development/which-impeller-is-right-for-your-cell-line-183538/

[13] Bernoulli Equation, Engineering ToolBox, 2003. Available at: https://www.engineeringtoolbox.com/bernouilli-equation-d_183.html

[14] Different Types of Pumps – Centrifugal Pumps Centrifugal Pumps, Process Industry Forum Available at: processindustryforum.com/article/different-types-pumps-centrifugal-pumps

[15] Pump and Pump system Glossary, Jacques Chaurette. Available at: https://www.pumpfundamentals.com/pump_glossary.htm#gl11

[16] Useful information on pump cavitation, Michael Smith Available at: https://www.michael-smith-engineers.co.uk/resources/useful-info/pump-cavitation

[17] The Logarithmic Spiral, Eric W. Weisstein, 1999. Available at: https://archive.lib.msu.edu/crcmath/math/math/l/l383.htm

[18] The Navier-Stokes Equations, Alessandro Bazzi, 2020. Available at: https://www.cantorsparadise.com/the-navier-stokes-equations-461f7453d79e

[19] Which Turbulence Model Should I Choose for My CFD Application?, Walter Fei, 2017. Available at: https://www.comsol.com/blogs/which-turbulence-model-should-choose-cfd-application/